Ocean Engineering 245 (2022) 110396

Contents lists available at ScienceDirect

Ocean Engineering

journal homepage: www.elsevier.com/locate/oceaneng

Probabilistic fatigue model for design and life extension of mooring chains, including mean load and corrosion effects

Erling N. Lone [a,*], Thomas Sauder [b,a], Kjell Larsen [a,c], Bernt J. Leira [a]

[a] Department of Marine Technology, Norwegian University of Science and Technology, Trondheim N-7491, Norway
[b] SINTEF Ocean, P.O. Box 4762 Torgarden, 7465 Trondheim, Norway
[c] Equinor ASA, Arkitekt Ebbells veg 10, 7053 Ranheim, Norway

ARTICLE INFO

Keywords:
Mooring line
S–N approach
Hindcast
Monte carlo simulation
Bootstrap

ABSTRACT

A probabilistic model for mooring chain fatigue damage is developed based on the S–N approach. The effects of mean load and corrosion condition on the fatigue capacity of the chains are included by adopting a parameterized S–N curve intercept parameter, and the model allows for the uncertainties and time dependencies of these to be addressed. Uncertainties in fatigue loads are also accounted for, including the annual variability which may be of importance in certain cases. Furthermore, the resulting model distinguishes between damage due to prior known loads and future unknown loads, to allow for reduced uncertainties in case that the load history is available from measurements or calculations. Measures are taken to ensure that the correlation between mean and cyclic loads is handled implicitly. A case study based on extensive hindcast-based simulations for a realistic mooring system is performed, and the respective effects of uncertainties in fatigue capacity, corrosion development and fatigue loads are presented and discussed.

1. Introduction

Fatigue assessment of mooring systems, as prescribed by relevant rules and standards (ISO 19901-7, 2013; DNV GL, 2018), involve considerable uncertainties with respect to both load and capacity. At the design stage, these uncertainties are handled by the use of large design fatigue factors (DFFs), in combination with (presumably) conservative assumptions. Examples of such assumptions are the joint direction and intensity of wind and waves, heading strategy for weathervaning units with active heading control, and the amount of marine growth and associated increase in mooring line drag coefficients. For life extension or in-service assessment during the operational lifetime, the analyses normally follow the same approach as that used during design. The numerical models and the input to the analyses may then be refined, but assumptions similar to those made at the design stage are still applied.

Current design codes target a maximum annual probability of mooring line failure in the range from 10^{-3} to 10^{-5} (DNV GL, 2018). Nevertheless, mooring lines historically tend to fail at an unreasonably high rate; Ma et al. (2013) discuss more than 20 incidents that occurred for permanent (long-term) mooring systems between 2001 and 2011; Kvitrud (2014) reports 15 mooring line failures for permanent and mobile units on the Norwegian Continental Shelf (NCS) between 2010 and 2013; Fontaine et al. (2014) report more than 40 failure events that occurred globally between 1997 and 2013. The root causes are diverse, however; almost half of the events described in Fontaine et al. (2014) were related to chain components and almost half of those were caused by fatigue and corrosion (Fontaine et al., 2014). Uncertainties in the dynamic loads and a lack of proper modeling of the effects that influence the capacity are likely contributors to these failures.

In order to better understand and quantify the fatigue capacity and degradation of mooring chains, a number of full scale fatigue tests have been performed in recent years, both for used chains retrieved after several years of service offshore (Fredheim et al., 2013; Gabrielsen et al., 2017; Ma et al., 2019; Gabrielsen et al., 2019) and for new chains of different sizes and material grades (Fernández et al., 2014; Zhang and Smedley, 2019; Fernández et al., 2019). These tests have shown that a reduction of the mean load increases the fatigue capacity (Zhang and Smedley, 2019; Fernández et al., 2019), and that the remaining fatigue life of used chains at low mean loads in some cases exceeds that expected for new chains at higher mean loads (Gabrielsen et al., 2019), but also that corrosion pits may have a significant detrimental effect (Gabrielsen et al., 2019; Ma et al., 2019). Inclusion of these effects seems crucial to enable improved estimates of mooring line fatigue life, both during design and for life extension of existing systems.

* Corresponding author.
E-mail address: erling.lone@ntnu.no (E.N. Lone).

https://doi.org/10.1016/j.oceaneng.2021.110396
Received 11 October 2021; Received in revised form 9 December 2021; Accepted 12 December 2021
Available online 23 January 2022

Lone et al. (2021) proposed an extended S–N curve formulation to include mean load and corrosion effects, by expressing the intercept parameter of the S–N model as a function of the mean load and a corrosion grade indicator. The coefficients of this model were estimated empirically from a data set that consisted of 125 full scale fatigue tests for both used (77 tests) and new chains (48 tests), tested at various mean loads and with various degrees of corrosion. They further demonstrated the impact on fatigue damage from considering realistic corrosion levels by comparison to the damage obtained from using the current design code (DNV GL, 2018). It was found that the negative effect of corrosion must be properly accounted for to avoid non-conservative fatigue damage estimates, in particular if the favorable effect of a low mean load is realized (or if the system is operated at high mean loads).

Knowledge of the load history may provide valuable insights to the fatigue loads that the system has been exposed to during operation. For instance, Russo et al. (2012) and Hørte et al. (2013) used measurements combined with numerical simulations to improve the estimates of wellhead fatigue damage accumulated during prior operations. However, measurements of mooring line tension tend to be inaccurate and biased (Brown et al., 2005). As an alternative, the load history may be established from measurements of position and motion of the floating unit, either in combination with a global performance model (Renzi et al., 2017) or as the basis for neural networks that are trained to predict mooring line tensions (Christiansen, 2014; Zhao et al., 2021). Methods for proper use of such load histories may reduce the uncertainties that were present for the design analyses, and thereby improve the predictions of future loads and remaining fatigue life in connection with life extension or reassessment.

Moan et al. (2005) showed that the annual variation of wave conditions causes a considerable variability for the structural fatigue loads of a ship-shaped production unit. This is likely to be the case also for mooring system fatigue, considering the similarities in prevailing environmental loads. As a consequence, the uncertainty in future fatigue damage may be underestimated if future fatigue loads are predicted based on simple extrapolation of prior loads, neglecting its variability. Addressing this variability may become particularly important if the prior loads are known only for a limited number of years (large uncertainties in estimation of the load distribution), or if the fatigue damage is predicted for a limited number of years (annual variability may be important).

In the present paper, we propose a new model for assessment of mooring chain fatigue, based on the extended S–N formulation proposed in Lone et al. (2021). A probabilistic approach is used, as it enables us to properly address the uncertainties both in loads and in the effects that influence the fatigue capacity of the components. Furthermore, a probabilistic model forms the necessary basis for a reliability-based integrity management of the mooring chains, as illustrated in Fig. 1. The resulting model distinguishes between the damage due to prior and future fatigue loads, respectively, to allow for utilization of load measurements or calculations from prior operation when available.

The paper is organized as follows. In Section 2, we develop the probabilistic model for the fatigue damage of mooring chains, including the effects of mean load, corrosion condition and fatigue load variability. In Section 3, we present a numerical mooring system model and simulations that have been performed based on a long series of hindcast data, and discuss some main results from these simulations in the context of the present study. By pretending that the simulations represent either load history measurements or possible realizations of such calculated prior to operation, we demonstrate and discuss the properties of the probabilistic model in a case study in Section 4. Some main conclusions of the study are given in Section 5.

2. Probabilistic model for fatigue damage

2.1. Fatigue damage with mean load and corrosion dependency

The S–N approach to fatigue of mooring chain is considered. Fatigue capacity is then expressed in terms of a stress-life (S–N) curve, defined as

$$N = A \cdot S^{-m} \tag{1}$$

where N is number of cycles to failure at constant stress range S, m is the slope parameter and A is the intercept parameter. The effects of mean load and corrosion condition are included by expressing the intercept parameter as a function of these parameters, as proposed in Lone et al. (2021):

$$\log A(\sigma_m, c) = b_0 + b_1 \cdot g_1(\sigma_m) + b_2 \cdot g_2(c) \tag{2}$$

where $\log(.)$ is the common logarithm, $(b_j)_{j\in\{0,1,2\}}$ are coefficients and $g_1(\sigma_m)$ and $g_2(c)$ are functions of the mean stress (σ_m) and a corrosion grade (c), respectively. The corrosion grade applied here is a custom scale from 1 (new chain or mild corrosion) to 7 (severe corrosion), see Lone et al. (2021) for details. Strictly, an error term should also be included to represent the predictive uncertainty of the regression model used to estimate the coefficients (Gelman and Hill, 2007). This is excluded for now and introduced later, without loss of validity for the derivations that follow.

By inverting the logarithm in (2) we get

$$A(\sigma_m, c) = 10^{\left(b_0 + b_1 \cdot g_1(\sigma_m) + b_2 \cdot g_2(c)\right)} \tag{3}$$

This formulation introduces a time-dependency to the capacity model, since (i) the mean load term depends on the stress process which fluctuates with time due to both short- and long-term variations in the environmental load process, and (ii) the last term represents degradation due to corrosion which is inherently a time-dependent process.

For variable amplitude loading, we adopt the Palmgren–Miner hypothesis on linear accumulation of the fatigue effect from each stress cycle. With the fatigue capacity described by (1) and (3), the Palmgren–Miner rule reads

$$D = \sum_i \frac{n_i}{N(\sigma_{m,i}, c_i)} = \sum_i \frac{n_i \cdot s_i^m}{A(\sigma_{m,i}, c_i)} \tag{4}$$

where D is referred to as the *fatigue damage* and n_i is the number of cycles with the stress range s_i, mean stress $\sigma_{m,i}$ and corrosion grade c_i.[1]

For a deterministic case, calculation of the fatigue damage caused by prior fatigue loads from the discrete sum in (4) is straightforward, and efficient in terms of computational cost once the stress cycles have been extracted from the load history. In the case of uncertain variables, computation of the fatigue damage distribution (by means of e.g., Monte Carlo simulation) requires multiple evaluations of (4), which leads to a significant increase in the computational cost. Furthermore, as it stands, it is not suitable for prediction of fatigue damage due to future, uncertain loads.

[1] When the mean load and corrosion dependent fatigue damage is expressed in terms of a single sum, it is assumed that pairs of stress range and associated mean stress are extracted and combined with the associated corrosion grade without binning them into a histogram. In practice, the number of cycles (n_i) will then be either 0.5 (for half cycles) or 1.0 (for full cycles). It may however easily be extended to a double or triple sum to handle empirical distributions represented by histograms in two (s, σ_m) or three (s, σ_m, c) dimensions.

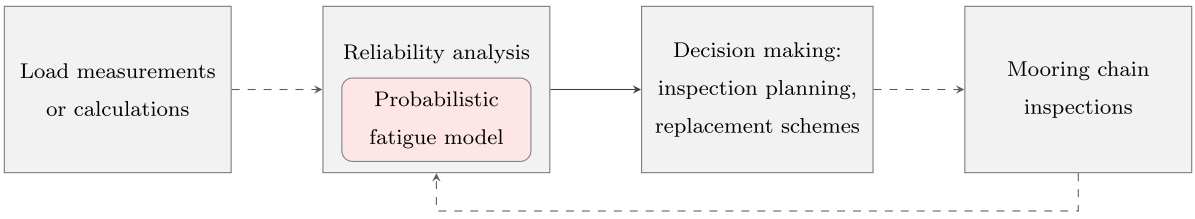

Fig. 1. Simplified illustration of reliability-based integrity management of mooring chains. The scope of the present study is indicated by the red box.

2.2. Time-variant formulation

We now consider a time interval $[\,t,\, t+\Delta t\,]$, which is sufficiently short for the intercept parameter to be constant. Within this interval, we express the number of cycles at each stress range level by the instantaneous probability density function of the stress range distribution, $f_S(s,t)$, such that $n_i = \nu(t) f_S(s_i,t)\Delta s \Delta t$, where $\nu(t)$ is the instantaneous cycle rate [s^{-1}]. The fatigue damage accumulated during the time period considered is then

$$D(t+\Delta t) - D(t) = \frac{\nu(t)}{A(\sigma_m(t), c(t))} \left\{ \int_0^\infty s^m f_S(s,t)\, ds \right\} \Delta t \tag{5}$$

It follows from the Palmgren–Miner rule that the total fatigue damage accumulated on the time interval $[\,0,\, t\,]$ is

$$D(t) = \int_0^t \frac{\nu(t)}{A(\sigma_m(t), c(t))} \left\{ \int_0^\infty s^m f_S(s,t)\, ds \right\} dt \tag{6}$$

By utilizing that the inner integral of (6) is the m-th moment of the stress ranges, $\mathrm{E}[S^m|t] = \int_0^\infty s^m f_S(s,t)\, ds$, and insertion of (3), we obtain

$$D(t) = \int_0^t \frac{\nu(t)\, \mathrm{E}[S^m|t]}{10^{\,\{b_0 + b_1 \cdot g_1(\sigma_m(t)) + b_2 \cdot g_2(c(t))\}}} dt \tag{7}$$

The underlying variables of this equation are $(m, b_0, b_1, b_2, \sigma_m(t), c(t), \nu(t), s(t))$, some of which are time-variant. In principle, they are all uncertain. Computation of this integral directly then requires the instantaneous, joint probability distributions of the uncertain variables to be known. This is hardly feasible in practice, since the environmental load process changes both with seasonal variations and during each day.

For the remainder of this paper we will assume that the S–N curve slope parameter (m) is fixed, and that all uncertainty associated with the S–N curve is represented by uncertainty in (one or more of) the coefficients of the intercept parameter (b_0, b_1, b_2).

2.3. Piecewise time-invariant formulation

The time period $[\,0,\, t\,]$ is now split into N_T intervals of duration T, and we introduce the following assumption: *the basic variables may be considered as piecewise time-invariant*. That is, within each of these intervals, the properties of the random variables are assumed to be constant. The time-variant formulation in (7) may then be written as a sum of time-invariant terms:

$$D(t) = \sum_{k=1}^{N_T} \frac{n_{0,k}\, \mathrm{E}[S^m]_k}{10^{\left(b_0 + b_1 \cdot g_{1,k}^* + b_2 \cdot g_{2,k}^*\right)}} \tag{8}$$

where $n_{0,k} = \nu_k \cdot T$ is the number of stress cycles and $(g_{j,k}^*)_{j\in\{1,2\}}$ are *representative* values of the mean load and corrosion functions in the k-th interval, respectively. Note that (8) does not necessarily represent an approximation compared to the time-variant formulation in (7), because (i) $\mathrm{E}[S^m]_k$ is calculated from the stress range distribution for the period considered, and (ii) for each period there exists values of $g_{1,k}^*$ and $g_{2,k}^*$ that would yield the same result as if the time-variant integral in (7) were computed. These may be referred to as *equivalent* values of g_1 and g_2. In practice, however, they will normally need to be approximated.

In many cases, corrosion may be assumed to be a slow process compared to the duration of the period, unless a very long time interval is considered (e.g., in the order of several years). A reasonable choice for the representative value of the corrosion grade function could therefore be its average value (that is, the time average of $g_2(c)$ over the k-th period). Alternatively, the value at the end of each period could be used as a more conservative choice. The impact of this choice is briefly discussed in connection with the case study in Section 4.

For the mean load function, it is convenient to distinguish between prior periods with known loads, and future periods with unknown loads. In the next subsection we will show how the representative value may be calculated for a period with known load history, which will be useful later for assessment of prior fatigue damage. The representative value for future periods will be addressed subsequently, in connection with prediction of the future, uncertain fatigue loads.

2.4. Representative mean load

If the load history for a given time period is known, a representative value for the mean load function may be calculated by requiring that each of the terms in (8) results in the same fatigue damage as (4) when calculated over the corresponding time intervals. For the k-th interval:

$$\frac{n_{0,k} \cdot \mathrm{E}[S^m]_k}{10^{\left(b_0 + b_1 \cdot g_{1,k}^* + b_2 \cdot g_{2,k}^*\right)}} = \sum_i \frac{n_i \cdot s_i^m}{10^{\left(b_0 + b_1 \cdot g_1(\sigma_{m,i}) + b_2 \cdot g_2(c_i)\right)}} \tag{9}$$

where the summation on the right hand side is over observations within the time period $[\,(k-1)T,\, kT]$, $n_{0,k} = \sum_i n_i$ is the total number of stress cycles and $\mathrm{E}[S^m]_k = \frac{1}{n_{0,k}} \sum_i n_i \cdot s_i^m$ is the m-th moment of S for this period. By replacing the corrosion grade function by its representative value, $g_2(c_i) = g_{2,k}^*$, and solving for $g_{1,k}^*$, we obtain:

$$g_{1,k}^* = -\frac{1}{b_1} \log \left[\frac{\sum_i n_i \cdot s_i^m \cdot 10^{-b_1 \cdot g_1(\sigma_{m,i})}}{n_{0,k} \cdot \mathrm{E}[S^m]_k} \right] \tag{10}$$

Provided that b_1 is fixed, Eq. (10) yields exactly the equivalent value of the mean load function. In case it is uncertain, its mean value may be used to provide a very good estimate of the equivalent value.

2.5. Fatigue load variables

We will now introduce two variables that will prove useful later.

$$Z = n_0 \cdot \mathrm{E}[S^m] \tag{11}$$

$$Z^* = n_0 \cdot \mathrm{E}[S^m] \cdot 10^{-b_1 \cdot g_1^*} \tag{12}$$

which will both be loosely referred to as "fatigue load" variables. The advantage of combining several variables into a single one is that any correlation between them is implicitly handled when represented by a probabilistic model. For the first variable (Z), the interdependency between n_0 and $\mathrm{E}[S^m]$ is intuitive, as they are both direct results of the cyclic stress process. If the mean load coefficient (b_1) is assumed fixed, it useful to also include the mean load effect in the fatigue load variable (Z^*). Strictly, the mean load function $g_1(\sigma_m)$ (or as here, g_1^*) is related

to the fatigue capacity.[2] However, since (i) it depends directly on the underlying load process and (ii) a high mean load has a negative impact on the fatigue capacity, it will be considered as a load variable in this context.

2.6. Annual fatigue damage

In the following, time intervals with duration $T = 1$ [year] is considered. This implies that each of the terms in (8) corresponds to the annual fatigue damage in the k-th year. We further distinguish between prior and future fatigue damage, such that

$$D(t) = \underbrace{\sum_{k=1}^{N_p} \frac{Z_k}{10^{\left(b_0 + b_1 \cdot g^*_{1,k} + b_2 \cdot g^*_{2,k}\right)}}}_{\text{Prior damage}} + \underbrace{\sum_{k=N_p+1}^{N_p+N_f} \frac{Z_k}{10^{\left(b_0 + b_1 \cdot g^*_{1,k} + b_2 \cdot g^*_{2,k}\right)}}}_{\text{Future damage}} \tag{13}$$

or in the case that the mean load coefficient (b_1) is assumed fixed:

$$D(t) = \sum_{k=1}^{N_p} \frac{Z^*_k}{10^{\left(b_0 + b_2 \cdot g^*_{2,k}\right)}} + \sum_{k=N_p+1}^{N_p+N_f} \frac{Z^*_k}{10^{\left(b_0 + b_2 \cdot g^*_{2,k}\right)}} \tag{14}$$

Here, N_p and N_f are the number of prior and future years, respectively, and the total number of years considered is $N_T = N_p + N_f$. The prior fatigue loads (Z and g^*_1, or Z^*) are assumed known, hence; uncertainty in prior fatigue damage is caused by uncertainties in the coefficients of the capacity model (b_0, b_1, b_2) and in the corrosion grade development ($g^*_{2,k}$). For future fatigue damage, the fatigue load variables are uncertain as well, and a natural question is how these may be predicted either from a known distribution or based on the knowledge of prior loads.

2.7. Uncertainty in future fatigue loads

We now assume that the long-term environment is represented by a stationary process, and that the annual distribution of waves is independent from year to year. Similarly, the annual distribution of wind is assumed independent from one year to another. We further introduce the following additional assumptions:

- *The system is operated the same way each year.* For instance, if the unit is operated with different winter and summer positions, these adjustments are assumed to be the same each years. For storage units with periodic changes in loading condition, the variations in draft are assumed to be similar from one year to another.
- *The mooring line properties do not change with time.* If a mooring line segment is replaced, it is assumed that the replacement does not affect the properties of the mooring line, and any changes in for instance marine growth (which affects the response through increased drag) are neglected.

Under these assumptions, the annual fatigue loads (Z or Z^*) are independent and identically distributed (i.i.d.) for any year k. A major benefit from considering *annual* distributions is that the seasonal variations in the environmental load process are implicitly accounted for.

The uncertainties in future fatigue loads may then be attributed to two main contributions:

1. Inherent variability, caused by the natural randomness of the environmental loads. This uncertainty is commonly referred to as *aleatory* uncertainty, and may be modeled by assigning a probability distribution to Z (or Z^*).
2. Uncertainty of the distribution parameters (for the probability distribution in the previous item), caused by lack of knowledge about the true parameters (e.g., because they need to be estimated from sparse data). This uncertainty is commonly referred to as *statistical* or *epistemic* uncertainty.

An additional source of uncertainty is introduced through the probabilistic modeling under item 1 above, as the selected distribution model may or may not represent the inherent variability well (this is commonly referred to as *model* uncertainty). Hence, selection of an appropriate distribution model is essential to properly account for the fatigue load variability. With the available data of prior fatigue loads as a basis, the choice of one distribution over another could be based on criteria such as the Akaike Information Criterion (AIC) or the Bayesian Information Criterion (BIC) (see e.g., Burnham and Anderson, 2002), although this is not addressed in the present paper.

Once a distribution model has been selected, the choice should generally be assessed by for instance goodness-of-fit (GoF) tests (see e.g., Ang and Tang, 2007). An example of this is given in Appendix A, where GoF tests are successfully performed for lognormal distribution of Z and Z^*, based on the data set presented in Section 3.

One way to address the epistemic uncertainty about the distribution parameters is to consider probability distributions for the parameters themselves. For some few probability distributions, exact sampling distributions for the parameters may be established (Ang and Tang, 2007; Bury, 1999). In the general case, however, they may be approximated by for instance Bayesian methods (O'Connor et al., 2007) or Bootstrap methods (parametric or non-parametric) (Efron and Tibshirani, 1986), possibly in combination (Efron, 2012).

Here, based on the results in Appendix A, we will consider the case that the annual variability may be represented by a lognormal distribution, and outline a parametric Bootstrap procedure to address the distribution parameter uncertainty.

2.7.1. Lognormal distribution of annual fatigue load

We will consider the special case that the annual fatigue load may be assumed to follow a lognormal distribution, denoted $Z \sim LN(.)$. For readability we will refer only to Z in this section, however, the discussion that follows is equally applicable also to Z^*.

The lognormal probability density function is

$$f_Z(z\,;\,\mu,\sigma) = \frac{1}{z \cdot \sigma \cdot \sqrt{2\pi}} \exp\left[-\frac{1}{2}\left(\frac{\ln(z)-\mu}{\sigma}\right)^2\right] \tag{15}$$

where $\ln(.)$ is the natural logarithm, and the distribution parameters (μ, σ) are respectively the mean value and standard deviation of the normal variate $\ln(Z)$. The cumulative distribution function (CDF) is

$$F_Z(z\,;\,\mu,\sigma) = \Phi\left(\frac{\ln(z)-\mu}{\sigma}\right) \tag{16}$$

where $\Phi(.)$ is the standard normal CDF. The true values of the distribution parameters are unknown, but may be estimated from a sample of observed values (e.g., from prior years). The maximum likelihood estimates (MLEs) (Bury, 1999) are

$$\hat{\mu} = \frac{1}{N}\sum_{i=1}^{N} \ln(z_i) \tag{17}$$

$$\hat{\sigma} = \sqrt{\frac{1}{N-1}\sum_{i=1}^{N} \left(\ln(z_i) - \hat{\mu}\right)^2} \tag{18}$$

where N is the sample size. These estimators yield unbiased point estimates for the distribution parameters (μ, σ), and correspond to the sample mean and standard deviation of $\ln(Z)$.

[2] For a structure with nonlinear restoring characteristics, such as a mooring line, the mean load will certainly influence the stress process as well. This is however implicitly represented in the stress range distribution, and therefore in $\mathrm{E}[S^m]$.

An attractive property of the lognormal distribution is that exact sampling distributions for μ and σ may be established from sampling theory for the normal distribution of $\ln(Z)$ (Bury, 1999). These could in turn be used to assess the effect of the epistemic parameter uncertainty on the prediction of future loads (and ultimately, on the fatigue damage). Here, however, we will instead consider a Bootstrap procedure that may be used for a Monte Carlo simulation to generate a sample distribution for future loads under parameter uncertainty. This approach is more generic (than using the theoretical sampling distributions) and may easily be adapted for use with probability distributions other than the lognormal.

A parametric Bootstrap for this purpose may be performed as follows (assuming that $\hat{\mu}$ and $\hat{\sigma}$ are estimated by (17) and (18) from a sample of prior loads of size $N = N_p$):

Step 1. Draw a sample of N_p realizations from $Z \sim LN(\hat{\mu}, \hat{\sigma})$.
Step 2. Fit distribution parameters $(\hat{\mu}_{BS}, \hat{\sigma}_{BS})$ to the sample from step 1, using (17) and (18).
Step 3. Repeat previous steps N_{BS} times to obtain a Bootstrap sample of the parameters, $(\hat{\mu}_{BS}^{(i)}, \hat{\sigma}_{BS}^{(i)}), i \in (1, \ldots, N_{BS})$.
Step 4. For each of the parameter sets from step 3, draw N_f realizations from $Z \sim LN(\hat{\mu}_{BS}^{(i)}, \hat{\sigma}_{BS})^{(i)}$.

In practice, this sampling scheme generates a (joint) Bootstrap distribution of (μ, σ), given the observed prior loads, and uses this to draw a sample of N_{BS} realizations of N_f i.i.d. future loads from a conditional distribution of Z. That is, the future loads are i.i.d. conditional on each realization of the distribution parameters. The procedure is analogous to drawing samples of future loads from a Bayesian posterior predictive distribution (Hastie et al., 2001, Section 8.4) except that here, an unweighted Bootstrap distribution is used for the parameters in lieu of a Bayesian posterior.

2.8. Summary of proposed model

To summarize the proposed model, we will illustrate how it may be used for fatigue assessment of a mooring chain component. Specifically, a procedure to estimate the fatigue damage distribution by means of Monte Carlo simulation (MCS) is outlined. Recall that the following assumptions have been made so far:

- Fatigue capacity is described by the S–N model in (1), with a mean load and corrosion dependent intercept parameter on the form defined by (3) (Section 2.1).
- For variable amplitude loads, the Palmgren–Miner hypothesis is adopted (Section 2.1).
- The S–N model slope parameter (m) is assumed fixed (Section 2.2).
- The underlying random variables may be considered as piecewise time-invariant (Section 2.3).
- The annual fatigue loads (prior and future) are i.i.d. (Section 2.7).

Furthermore, to enable a concise illustration of the approach, the following additional assumptions are introduced:

- All uncertainty associated with the fatigue capacity is represented by a random b_0 coefficient, whereas the (b_1, b_2) coefficients are assumed fixed. This simplification implies that the annual fatigue load may be conveniently represented by Z^*. Note that the effect of this assumption is addressed as part of the case study in Section 4.
- The annual fatigue load (Z^*) follows a lognormal distribution. This implies that the estimators and the bootstrap procedure described in Section 2.7.1 may be used.

Fig. 2 shows a flow chart for the suggested procedure, given these latter assumptions, using MCS to generate N_{MC} realizations of the fatigue damage calculated from (14). Selected aspects of this workflow are briefly described and discussed in the subsequent paragraphs.

Scenarios. Two main scenarios are addressed. The first is *design verification* (or, any fatigue assessment performed prior to operation). In this scenario, all fatigue loads are future loads. Hence, we have $N_p = 0$ and $N_T = N_f$. Estimation of Z^* distribution (type and parameters) could then be based on possible realizations of annual fatigue loads, e.g., from numerical simulations for N years of historic hindcast data – similar to those that will be presented in Section 3. The second scenario is *in-service assessment* after N_p years of operation. Load history is then assumed available for $N = N_p$ prior years, and the objective is to estimate the fatigue damage distribution after a total of $N_T = N_p + N_f$ years. In this scenario, the prior fatigue loads (denoted z_p^* in the figure) are used both to estimate the Z^* distribution parameters, and as deterministic loads for the prior fatigue damage.

Fatigue capacity. For a given chain component, the b_0 term is considered as random but time-invariant, since the time-dependency of the fatigue capacity is handled by the mean load and corrosion grade terms of the intercept parameter. Each realization of the fatigue damage therefore requires only one realization of b_0. Also, note that with b_1 and b_2 fixed, the mean load and corrosion grade effects on the capacity may be regarded as deterministic functions of random loads, expressed through g_1^* and g_2^*.

Fatigue loads. Each realization of the fatigue damage after N_T years requires N_f realizations of Z^*. This may equivalently be understood as drawing a single realization of N_f i.i.d. random variables, each representing the fatigue load in one of the future years.

Corrosion model. The probabilistic corrosion model could be based on one or more underlying random variables. The main point at this stage is that for each realization of the corrosion grade history, it should enable calculation of the representative value of $g_2(c)$ (i.e., g_2^*) for each of the N_T years. An example of a simple probabilistic model for this purpose is presented and applied for the case study in Section 4.

Fatigue damage distribution. The fatigue damage sample distribution is the main result and output from the workflow. Strictly, computation of (14) yields the accumulated fatigue damage after the last of the N_T years (i.e., a sample of size N_{MC} is obtained). However, using the samples drawn in the MCS, computation of the fatigue damage by the end of each of the N_T years is available at practically no additional computational cost, resulting in a sample of size $N_{MC} \times N_T$.

Reliability analysis. A main goal in applying a probabilistic approach to fatigue is to enable a reliability analysis, to calculate the probability of (fatigue) failure. This requires a limit state function to be defined (Melchers and Beck, 2018), and this will normally require additional probabilistic models that are not addressed in the present study. Examples of such are model uncertainties that account for the uncertainty in the Palmgren–Miner rule (Wirsching and Chen, 1988) and uncertainties and possible bias in load measurements or simulations. The figure indicates how the workflow could be integrated as part of a reliability analysis that is based on MCS, with the fatigue damage sample distribution as direct input. In a more general case, however, the limit state function could be expressed as a direct function of all underlying random variables to allow for alternative calculation methods such as FORM or SORM (Melchers and Beck, 2018). The results from the reliability analysis may in turn be used as the basis for decision making, such as for instance inspection planning and chain replacement schemes.

A note on the need for the additional assumptions. Although convenient, the additional assumptions that were introduced are not *strictly* necessary. Firstly; if the b_1 coefficient is random, the following adjustments could be done: the sensitivity for g_1^* to variations in b_1 should

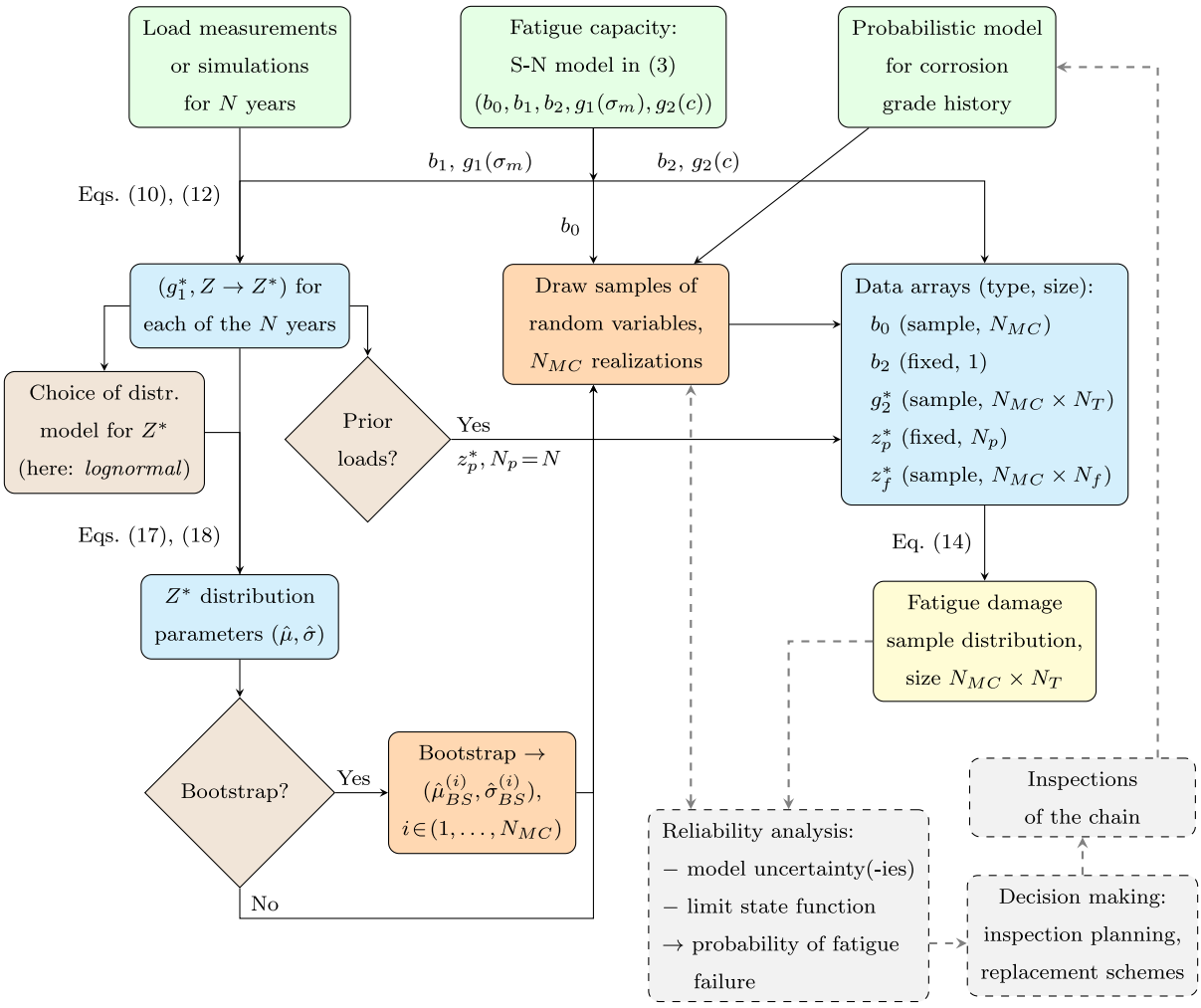

Fig. 2. Fatigue damage distribution analysis by Monte Carlo simulation. Gray boxes with dashed arrows indicate how the workflow could be integrated as part of a reliability analysis for decision making and inspection planning.

be assessed, and future loads should be modeled through the joint distribution of g_1^* and Z instead of the marginal distribution of Z^*. Alternatively, if the annual variability of g_1^* is shown to be reasonably small, it could be set to a fixed (and possibly conservative) value to allow for the marginal distribution of Z to be used. Secondly; if the annual fatigue load is found to follow a different probability distribution (other than the lognormal), different estimators for its distribution parameters would be used and an adjusted Bootstrap procedure (or alternative approaches) to address the epistemic uncertainty of these parameters could be considered.

Computational cost. As the model relies on load measurements and/or simulations for several years of operation, the computational cost of establishing the probabilistic fatigue load model will generally be significant. Important factors affecting the exact computational effort are the sources from which the fatigue loads are obtained and the number of prior years considered. However, once the probabilistic model for Z (or Z^*) is established, a fatigue damage sample distribution may be generated at a low computational cost. For example, using custom-written Python code implementing the workflow illustrated in Fig. 2, the following performance was obtained on a standard commercial laptop[3]: with $N_p = 0$ and $N_f = 15$, a fatigue damage sample of size $N_{MC} = 10^5$ was generated in less than 0.5 s, and a sample of size $N_{MC} = 10^6$ was generated in less than 2 s.

3. Basis for the case study

The basis for the case study in Section 4 is now presented. Mooring line responses are computed by numerical time domain simulations based on environmental data from a hindcast series that covers 61 years. Results for response variables of interest (g_1^*, Z, Z^*) are presented and discussed.

3.1. Description of platform and mooring system

A semi-submersible production unit operating at 300 m water depth in the Norwegian Sea is considered. The platform has six columns, two pontoons with length 102.4 m at a distance of 96 m, a draft of 25 m and a total displacement of 84848 metric tonnes. It is permanently moored by a spread mooring system that consists of 16 lines in clusters of four (Fig. 3). The fairleads are located at a radial distance of approximately 68 m from the unit center, 8.8 m below the still water level. The mooring pattern is slightly asymmetric, with shorter lines towards east.

[3] The laptop used is equipped with a Quad-Core Intel Core i7-8650U CPU @ 1.90 GHz.

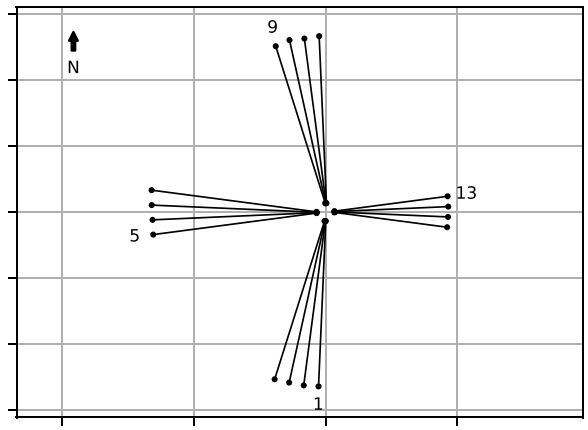

Fig. 3. Horizontal projection of mooring system.

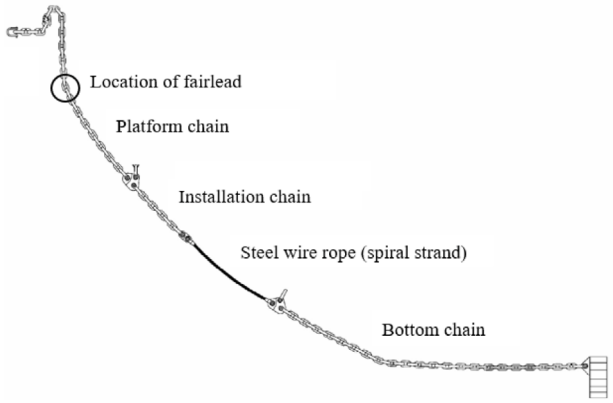

Fig. 4. Mooring line composition. Not to scale.

A lower pretension[4] is applied for the westward cluster to reduce the extreme loads in these lines, as they point towards the dominating wave directions. All lines are composed of a catenary chain-wire-chain configuration, with studless chain for the upper and lower segments, and steel wire rope in-between (Fig. 4):

- Chain segments: studless R4 chain, with a nominal diameter of 142 mm and a nominal (tabulated) MBL of 18033 kN.
- Steel wire rope: sheathed spiral strand wire, with a diameter of 156 mm (incl. 20 mm plastic sheathing).

Anchor positions applied in the numerical model are based on field measurements, and the lengths of the platform chain segments have been adjusted to obtain pretensions close to those measured on site.

3.2. Environmental data

Environmental conditions are based on a hindcast data series for the Norwegian Sea (Reistad et al., 2011), representing simultaneous observations of wave and wind conditions over successive 3 h. Each sea state is characterized by (i) significant wave height, wave spectral peak period and mean direction for total sea, and (ii) wind velocity and direction. Note that it is also possible to extract sea state parameters for wind sea and swell, which enables modeling of the two wave systems from separate directions instead of applying a single wave spectrum for the total sea. This is assumed to be of limited importance for the semi-submersible unit considered, since the wave load magnitude is not that sensitive to the angles of attack (which would not necessarily be the case for a ship-shaped and weathervaning unit, as heading towards one wave system may then increase the wave loads induced by the other wave system).

For the present study, 61 full years of hindcast data from 1958 through 2018 have been applied. In total, this constitutes 178420 sea states of 3-hour duration. Some main characteristics of the hindcast series are visualized in Figs. 5–7, showing that:

- There is considerable annual variation in the intensity of the largest sea states (Fig. 5).
- The most frequent wave directions are from southwest and west, followed by north and northwest (Fig. 6). Very few of the sea states are with waves from east and southeast.
- Wind and total sea wave directions appear to be fairly uncorrelated for the lowest sea states, but with an increasing and strong correlation for increasing sea state intensity (Fig. 7). For the most severe sea states, wind and waves act roughly in the same direction.

In addition to waves and wind, current has been included based on a simple relation to the wind velocity, in accordance with DNV GL (2019): $U_c = 0.20 + 0.05 \cdot U_w$, where U_c and U_w are the current and wind velocities, respectively. Current direction is rotated 15° clockwise from the wind direction.

3.3. Method description

Tension–tension fatigue of a chain component located at the fairlead is considered. Mooring line responses are computed with time domain simulations, using a decoupled approach[5]:

1. Floater motions are simulated with a quasi-static representation of the mooring line forces.
2. The motion from step 1 is imposed on finite-element (FE) models of the mooring lines of interest, to obtain time series of mooring line axial tension that include geometric non-linearities and dynamic effects such as drag and inertia.

The first step is performed with the computer program SIMO (SINTEF Ocean, 2019a), which solves the nonlinear and dynamic equation of motion in time domain with excitation from waves, wind and current. Waves are described by the double-peaked Torsethaugen wave spectrum (DNV GL, 2019; Torsethaugen and Haver, 2004), assuming long-crested (unidirectional) sea. Wind speed fluctuations are modeled by the NPD/ISO wind spectrum (ISO 19901-1, 2015), whereas the current velocity is assumed constant. The quasi-static representation of the mooring lines implies that the nonlinear restoring characteristics of the lines are accounted for, whereas dynamic effects due to drag and inertia are neglected. The numerical model includes frequency dependent hydrodynamic coefficients for first and second order (wave drift) wave excitation based on potential theory, where the latter have been adjusted empirically through comparison to model test results. Wave–current interactions are represented through a simplified wave drift damping formulation, and frequency dependent added mass and potential damping are represented by retardation functions. Wind and current loads are included by means of quadratic load models. Additional damping is provided through linear and quadratic damping matrices, representing viscous damping due to columns and pontoons

[4] Pretension is defined as the tension in the mooring line, at the fairlead, when there are no environmental loads acting on the unit or on the mooring lines.

[5] See e.g. Ormberg and Larsen (1998), Ormberg et al. (1998) for a discussion on the differences between coupled and decoupled (referred to as "separated" in the first reference) simulation of mooring line response.

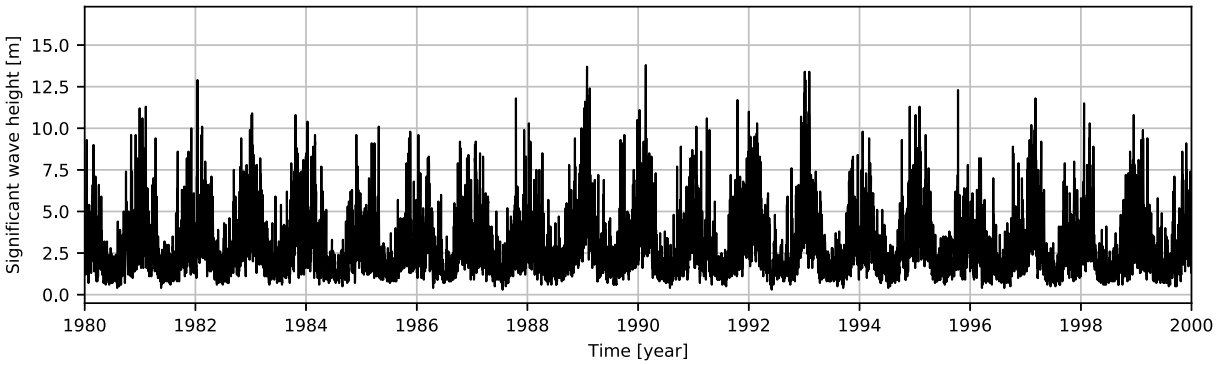

Fig. 5. Excerpt of hindcast series for significant wave height, years 1980–2000.

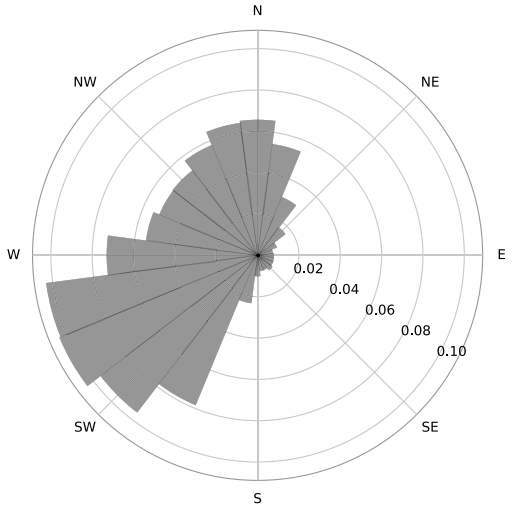

Fig. 6. Relative frequency of occurrence for total sea mean wave direction (coming from), years 1958–2018.

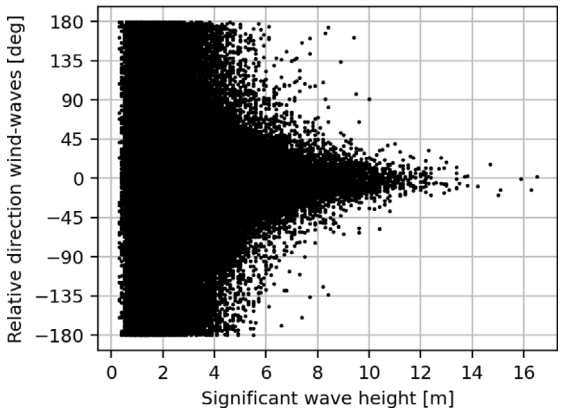

Fig. 7. Relative direction of wind-waves vs. significant wave height, years 1958–2018.

Table 1
Mooring lines considered for dynamic simulation with RIFLEX.

Line	Cluster	Pretension [% MBL]
1	South	12.0
5	West	10.9
9	North	11.9
13	East	12.1

as well as damping contributions induced by mooring lines and risers. Quasi-static models of the risers are included to ensure that their stiffness contributions are accounted for.

The second step is performed with RIFLEX (SINTEF Ocean, 2019b), using bar elements for the mooring line FE model. Drag, added mass and inertia effects on the mooring line responses are then accounted for, including the effects of marine growth which are represented through increased drag coefficients and unit mass in line with DNV GL (2018). In the present study, one mooring line from each cluster is considered for the dynamic simulation, as listed in Table 1. Examples of the axial tension time series obtained for two of these lines are shown in Fig. 8, for one 3-hour sea state. Time series of nominal stress are obtained from dividing axial tension response by the nominal cross section area of the mooring chain links. Stress cycles are then extracted by rainflow counting, using the algorithm from ASTME E1049-85 (ASTM International, 2017, Section 5.4.4).

For each of the 3-hour sea states, a simulation of 3-hour duration is conducted. Steinkjer et al. (2010) showed that this may imply considerable statistical uncertainty for the short-term fatigue damage of similar slender structures. This uncertainty is not addressed in the current study for the following reasons:

- All 3-hour sea states are simulated, without any kind of blocking to reduce the number of simulations. It is therefore reasonable to assume that the resulting statistical uncertainty is small when the fatigue damage is summed up over a year. This is in line with the findings in Steinkjer et al. (2010).
- For the present study, the simulations are assumed to mimic a realization of measured load histories. Hence, any statistical uncertainty arising from the stochastic realizations of short-term conditions may be considered irrelevant.

3.4. Results from hindcast-based simulations

For each of the years considered in the simulations, the representative mean load (g_1^*) and the fatigue load variables (Z, Z^*) have been calculated from the (annual) joint, empirical distributions of stress cycles and mean load. For these calculations, the mean load function is $g_1(\sigma_m) = \lambda_m$, where λ_m is the mean load expressed as percentage of the nominal MBL. The relevant S–N curve coefficients have been kept fixed at $m = 3$ and $b_1 = -0.0507$ (Lone et al., 2021).

Statistics for these annual response values are presented in Table 2. The mean value of the representative mean load is seen to be higher than the pretension (see Table 1) for all mooring lines except line 13 (East). This may be explained by considering the directions of the lines. For waves from the dominating wave directions (western sectors), the platform is offset towards east, thereby reducing the mean tension in the eastern cluster. Hence, for line 13, the majority of the fatigue loads are accumulated at mean loads below the pretension. The

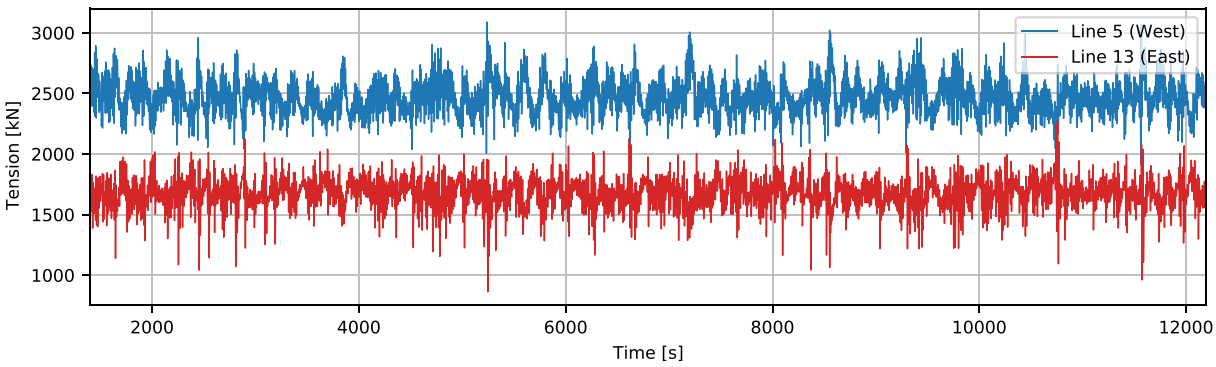

Fig. 8. Example of 3-hour axial tension time series for chain components located at fairlead. Significant wave height 10.7 m, wave spectral peak period 14.3 s and wind velocity 23.4 m/s. Wind and waves from west.

Table 2
Annual load statistics, based on simulations for 61 years (1958–2018).

Variable, Mooring line	Cluster	Mean	CoV	Skewness	Excess kurtosis	Fitted parameters[a]	
						$\hat{\mu}$	$\hat{\sigma}$
g_1^* [% MBL]							
1	South	12.8	0.04	0.17	−0.71		
5	West	12.1	0.02	0.96	1.46		
9	North	12.6	0.04	−0.17	−0.64		
13	East	11.2	0.03	0.31	0.20		
$Z = n_0 \cdot \mathrm{E}[S^m]$ [MPa^3]							
1	South	8.53×10^7	0.26	0.85	1.31	18.23	0.257
5	West	6.20×10^7	0.38	1.13	1.31	17.88	0.364
9	North	7.53×10^7	0.24	0.49	−0.72	18.11	0.235
13	East	9.20×10^7	0.33	1.04	1.06	18.29	0.316
$Z^* = n_0 \cdot \mathrm{E}[S^m] \cdot 10^{-b_1 \cdot g_1^*}$ [MPa^3]							
1	South	3.82×10^8	0.29	1.20	2.92	19.72	0.282
5	West	2.59×10^8	0.41	1.28	1.76	19.30	0.389
9	North	3.31×10^8	0.25	0.45	−0.87	19.59	0.252
13	East	3.36×10^8	0.30	0.93	0.71	19.59	0.287

CoV: Coefficient of Variation.
[a]Lognormal distribution parameters estimated by Eqs. (17) and (18).

other lines are to a larger degree orientated towards the dominating wave directions, and therefore accumulate most of the fatigue loads at mean loads above their pretensions. The largest difference between pretension and representative mean load is seen for line 5 (West), which points in the statistically most exposed direction.

The highest mean annual fatigue load (Z) is obtained for mooring line 13 (East), which experiences large tangential motions for the upper end of the mooring line and therefore large cyclic loads due to its orientation along the axis of the dominating wave directions. This is also the case for line 5 (West), but the larger line length gives a softer stiffness characteristics despite the higher mean loads, effectively reducing the cyclic loads.

When the fatigue load is combined with the mean load effect (Z^*), the highest mean value is obtained for line 1 (South). The significance of this result is the following. If mooring line fatigue were assessed without accounting for the mean load effect, assuming similar corrosion conditions for all lines, the *eastern* cluster would be the most critical due to the higher cyclic loads (as expressed through Z). By accounting for the mean load effect on fatigue capacity, using Z^*, the relative importance of the clusters is altered and the *southern* cluster becomes the most critical. This is consistent with the findings in an initial study for this unit, as reported in Lone et al. (2020), and underlines the need to account for mean loads to properly identify the critical mooring lines with respect to fatigue.

Annual variability is represented by the coefficient of variation (CoV). For representative mean load, the CoV is seen to be low for all mooring lines. A considerably larger variability is observed for the annual fatigue load, with the highest CoV at 37% for line 5. When fatigue load is combined with the mean load effect, the CoV for line 5 increases to 40%. Line 13 is the only mooring line that experiences a reduction in the CoV when the mean load effect is included, indicating a negative correlation between g_1^* and Z for this line. This is confirmed by the scatter plots in Fig. 9 for lines 5 and 13, and the associated correlation coefficients are estimated to 0.86 and −0.76, respectively. The orientation of the southern and northern clusters causes a weaker correlation between g_1^* and Z for lines 1 and 9, with correlation coefficients at 0.39 and 0.22, respectively. This is because a larger share of the fatigue loads for these lines are induced by waves acting less along their respective directions, with a more varying effect on the mean loads. As an example, for line 1; frequent waves from the southwestern sectors will induce mean loads that are higher than the pretension, whereas waves from the western sectors (which are also quite frequent) will have a lesser impact in this regard.

The results statistics in Table 2 also show that the annual fatigue load variables (Z, Z^*) are positively skewed, and visual inspection of histograms (not presented here) indicate that they could be well represented by a lognormal probability distribution. Based on goodness-of-fit tests it is concluded that the lognormal distribution is acceptable for Z and Z^* for all four mooring line. For details and test-of-fit results, see Appendix A.

Only two of the mooring lines will be considered for the case study, to limit the amount of results. As the objective is to demonstrate the properties of the probabilistic model, the following lines are selected:

- Line 5 (West), on the basis of the high annual fatigue load variability.

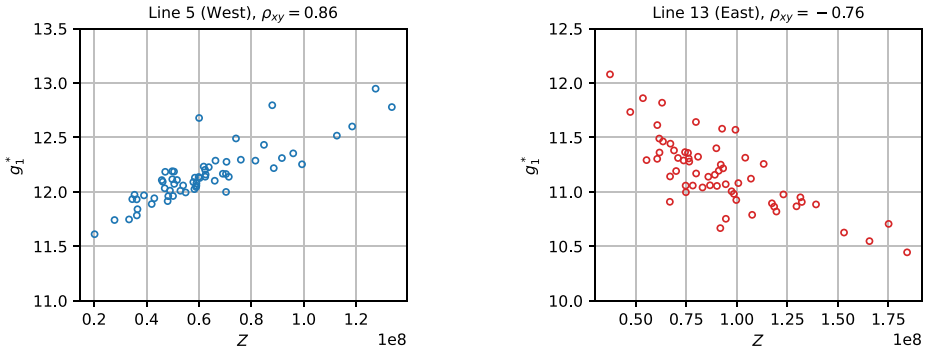

Fig. 9. Scatter plot of g_1^* vs. Z (annual values) for lines 5 (left) and 13 (right). Correlation coefficients are given in figure titles.

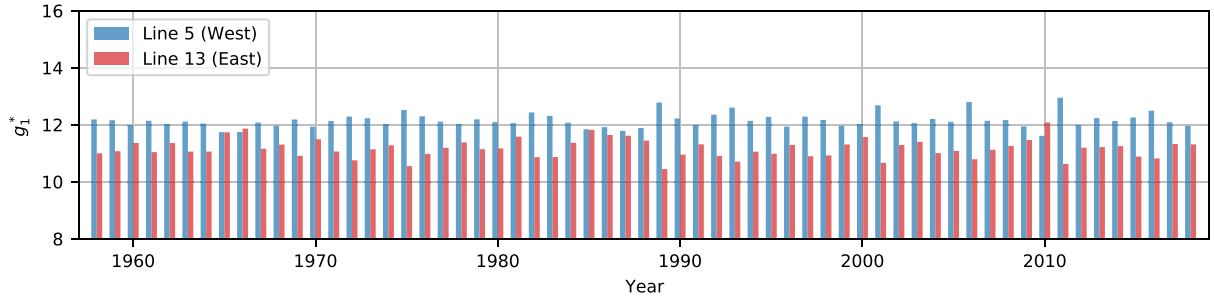

(a) Representative mean load, g_1^*.

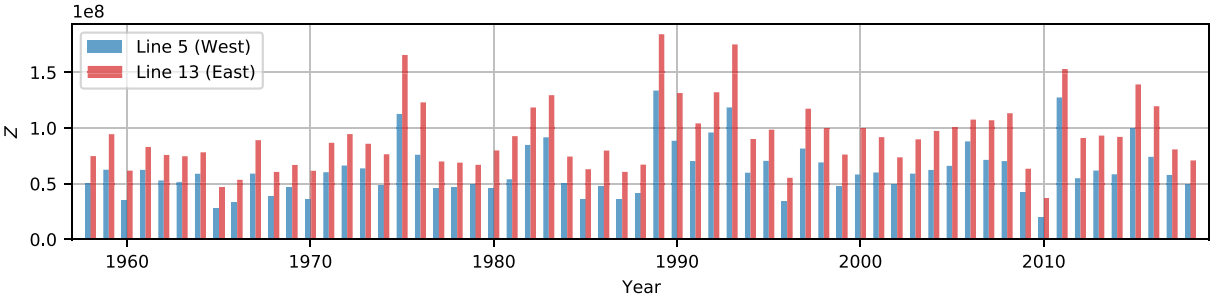

(b) Fatigue load, $Z = n_0 \cdot \mathrm{E}[S^m]$.

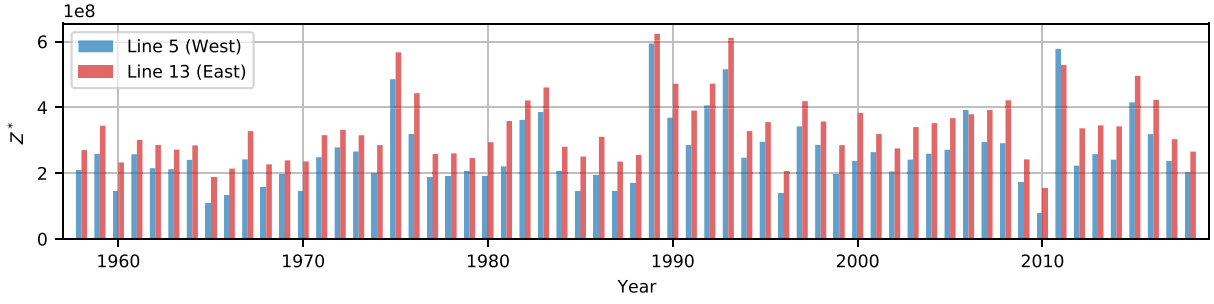

(c) Fatigue load combined with mean load effect, $Z^* = n_0 \cdot \mathrm{E}[S^m] \cdot 10^{-b_1 \cdot g_1^*}$.

Fig. 10. Annual representative mean load and fatigue load variables for mooring lines considered in the case study.

- Line 13 (East), on the basis of mean load properties that deviate from the those of the other lines.

Bar plots of g_1^*, Z and Z^* for the selected lines are shown in Fig. 10, for all 61 years. The limited variability of the representative mean load is evident from the plot, as is also the distinct variability of the fatigue loads. For line 5, the maximum values of Z and Z^* are more than six and seven times higher than the respective minimum values. For line 13, the corresponding ratios of maximum to minimum values are around five and four, respectively.

Note that the case study selection excludes line 1 (South), for which the highest combined fatigue and mean load effect is observed (i.e., highest mean value of Z^*). This does not limit the value of the case study, as this line exhibits load properties that are within the bounds of the selected lines.

4. Case study

In this section, we apply the probabilistic model established in Section 2 to the data set presented in Section 3, to demonstrate the properties of the model. Uncertainties in fatigue capacity, corrosion grade and fatigue loads are addressed one at a time, to present and discuss their respective effect on the fatigue damage uncertainty.

The scenario considered is that fatigue damage is accumulated over 15 years, starting in 1980. Initially, the fatigue loads during all 15 years are assumed known, which enables us to isolate the effects of uncertainty in fatigue capacity and corrosion grade, respectively. We then consider two scenarios with uncertain fatigue loads; one relevant for design verification, and one relevant for in-service assessment after ten years of operation.

Monte Carlo simulation (MCS) is used extensively throughout the case study, to simulate realizations of the uncertain variables and ultimately evaluate the accumulated fatigue damage represented by the piecewise time-invariant summation in either (13) or (14). The procedure generally follows that outlined in Section 2.8 (Fig. 2), except for the initial case considering uncertainty of the fatigue capacity model. The MCS for this particular case is described in the relevant subsection. A sample size of $N_{MC} = 10^5$ is generated for all simulations unless otherwise noted.

For the entire case study we will use the mean load function $g_1(\sigma_m) = \lambda_m$, where λ_m is the mean load in % MBL, and the corrosion grade function $g_2(c) = c$.

4.1. Uncertainty in fatigue capacity

We start by considering only uncertainty in the fatigue capacity, as defined by the intercept parameter in (3). Specifically, we will assess the respective importance of the *predictive* and the *inferential* uncertainties in the S–N regression model established in Lone et al. (2021). The former uncertainty relates to the standard error of the regression model (residuals), whereas the latter relates to the standard errors of the estimated regression coefficients (Gelman and Hill, 2007). To address these, we temporarily introduce an error term (ϵ) to the intercept parameter, so that the equation describing the fatigue capacity becomes

$$A(\sigma_m, c) = 10^{\left(b_0 + b_1 \cdot g_1(\sigma_m) + b_2 \cdot g_2(c) + \epsilon\right)} \tag{19}$$

and update the denominator of the fatigue damage summation in (13) accordingly. The regression analysis performed in Lone et al. (2021) has been rerun for the present study, to calculate the standard errors of the $(b_j)_{j\in\{0,1,2\}}$ coefficients (Table 3). Their covariance matrix is

$$\boldsymbol{\Sigma} = \begin{bmatrix} 7.770\times10^{-3} & -3.829\times10^{-4} & -4.453\times10^{-4} \\ -3.829\times10^{-4} & 2.046\times10^{-5} & 1.714\times10^{-5} \\ -4.453\times10^{-4} & 1.714\times10^{-5} & 5.612\times10^{-5} \end{bmatrix} \tag{20}$$

and the corresponding correlation matrix is

$$\boldsymbol{\rho} = \begin{bmatrix} 1. & -0.96 & -0.67 \\ -0.96 & 1. & 0.51 \\ -0.67 & 0.51 & 1. \end{bmatrix} \tag{21}$$

Two cases are simulated, using MCS with the procedure outlined in Gelman and Hill (2007, Chapter 7): (i) predictive uncertainty only, that is, random error (ϵ) and deterministic b_j-coefficients, and (ii) combined predictive and inferential uncertainty, that is, random error and random b_j-coefficients. For each realization in this MCS, we draw one value for each of the random variables in the capacity model and calculate the fatigue damage by (13), assuming that simultaneous observations of Z and g_1^* through the $N_T = N_p = 15$ years from 1980 to 1994 are deterministic and known. Note that for consistency, the annual representative mean loads (g_1^*) for these years are first recalculated for each realization of the mean load coefficient (b_1), using (10) with the joint, empirical distributions of stress ranges and mean loads. The corrosion grade is assumed to evolve deterministically from $c = 1$ at the beginning of 1980 to $c = 4$ at the end of 1994, with a linear development.

Table 3
Probabilistic description of fatigue capacity variables.

Variable	Mean value	Standard deviation	Distribution	Note
b_0	12.249	0.088	Normal	[a]
b_1	−0.0507	0.0045	Normal	[a]
b_2	−0.106	0.0075	Normal	[a]
ϵ	0	σ_ϵ	Normal	
σ_ϵ	0.170	–	Fixed	[b]

[a] Multivariate normal with covariance matrix given in (20).
[b] Standard error of the capacity model.

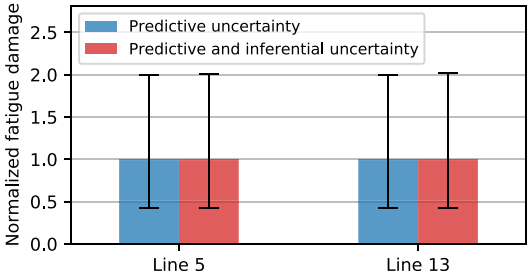

Fig. 11. Importance of predictive vs. inferential uncertainty of fatigue capacity model. Expected value and 95% confidence interval of fatigue damage sample distributions. For each of the mooring lines, the values are normalized wrt. expected damage for the case with predictive uncertainty only.

Results are shown in Fig. 11, for mooring lines 5 (West) and 13 (East). Uncertainty in fatigue capacity is dominated by the predictive uncertainty, and the mean value and the upper limit of the 95% confidence interval increase by less than 1% when inferential uncertainty is included as well. The small effect of the inferential uncertainty is primarily caused by the strong correlation between the regression coefficients; a low value of b_0 is likely to be combined with high values of b_1 and b_2, as seen from Fig. 12.

It should noted that the standard error of the model (σ_ϵ) is here assumed deterministic for both cases. Strictly, it is distributed according to $\hat{\sigma}_\epsilon\sqrt{(n-l)/\chi^2_{n-l}}$, where $\hat{\sigma}_\epsilon = 0.170$ is the estimated standard error, $n = 125$ is the number of fatigue tests included in the regression analysis, $l = 3$ is the number of estimated coefficients and χ^2_{n-l} is a chi-square distribution with $(n-l)$ degrees-of-freedom. However; if this were included in the MCS, the upper bound of the confidence interval would increase only by around 1%.

A limitation in the assessment performed here is that mean loads and corrosion grades are assumed deterministic. Hence, interactions between uncertainties in these and the uncertainties in (b_1, b_2) are neglected. Considering the negligible impact of the inferential uncertainty, however, it is reasonable to assume that this would be of limited importance.

A convenient simplification of the model is then to omit the error term in (19) and include this uncertainty in the b_0 coefficient instead by letting $\sigma_{b_0} = \sigma_\epsilon$, while assuming deterministic (b_1, b_2) coefficients with values fixed at the respective mean values in Table 3. Furthermore, with b_1 fixed, the variable Z^* may be used to represent the fatigue loads.

In other words, the fatigue capacity may be modeled by $b_0 \sim N(12.249, 0.170^2)$, $b_1 = -0.0507$ and $b_2 = -0.106$. Since the fatigue damage is proportional to 10^{-b_0}, it follows that the CoV of fatigue damage due to uncertainty in capacity alone is 0.41.

4.2. Uncertainty in corrosion grade

In order to obtain proper corrosion grade estimates for mooring chains, the components must be inspected. A priori, the only available

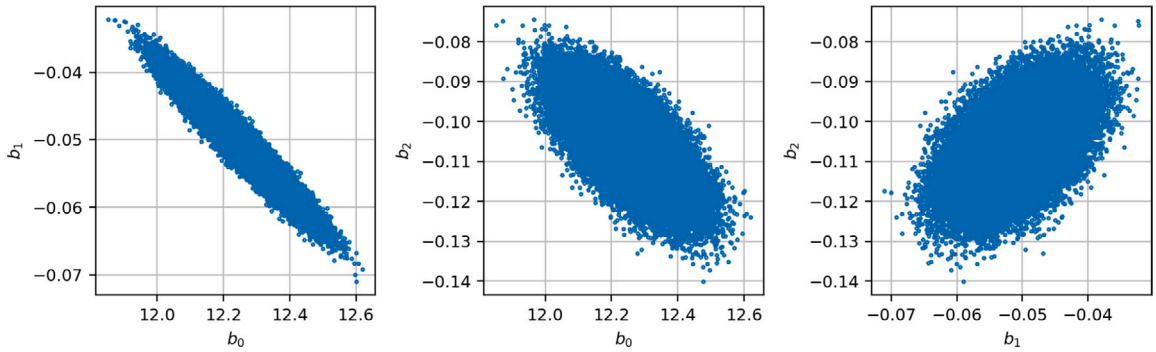

Fig. 12. Simulated values of the S–N curve coefficients; b_1 vs. b_0 (left), b_2 vs. b_0 (center) and b_2 vs. b_1 (right).

Table 4
Cases for assessment of corrosion grade uncertainty.

Case	C_{end}	η	Description
I	4	1	Reference case
IIa	$U(1,7)$	1	Linear corrosion grade development
IIb	$U(1,7)$	2	Slow initial corrosion grade development
IIc	$U(1,7)$	0.5	Fast initial corrosion grade development

information is that the grade is bounded by the value at installation ($c = 1$) and the upper limit of the corrosion grade scale ($c = 7$). Even if the grade at a given point in time is known, the fatigue damage is also affected by its development from 1 to this value, as a more rapid increase in the corrosion grade will result in a higher fatigue damage compared to a slower development. A detailed or complex model of the corrosion development is beyond the scope of the present study. For simplicity, we will assume that the representative value of the corrosion grade function in the k-th year may be expressed as

$$g^*_{2,k} = c_k = 1 + (C_{\text{end}} - 1) \cdot \left(\frac{k - a}{L}\right)^{\eta} \tag{22}$$

where L is the service life, C_{end} is the corrosion grade at the end of the service life, η is an exponent that determines the shape of the time history, and $a \in [0, 1]$ controls which value is taken as the representative one. For example, $a = 0.5$ implies that the corrosion grade is represented by its value halfway through that year (which here corresponds to the average value of $g_2(c)$), whereas $a = 0$ means that the value at the end of the year is used. Examples of time histories with three different values of η are shown in Fig. 13. In the following, η is assumed to be deterministic (i.e., the shape of the time history is fixed), the service life L is assumed to be 15 years and C_{end} is assumed to follow a uniform distribution with support $[1, 7]$, denoted $C_{\text{end}} \sim U(1, 7)$. One could argue that a corrosion grade of 1 after 15 years is unlikely, and that bounds $[2, 7]$ would be more appropriate. However, as the main purpose here is to illustrate the effect on fatigue damage uncertainty, this is disregarded.

Cases for assessing the effect of corrosion grade uncertainty are listed in Table 4. A deterministic fatigue load history is used for all these cases, and the coefficients of the fatigue capacity model are assumed fixed at their mean values. Case I with fixed final corrosion grade then yields a deterministic fatigue damage, and serves as a reference case. Uncertain corrosion grade is introduced for case IIa, whereas the effect of the shape of the corrosion grade development (through η) is addressed by cases IIb and IIc. Note that $\mathrm{E}[C_{\text{end}}] = 4$ for all the listed cases, and the temporal expected value of $g^*_{2,k}$ matches the respective time histories in Fig. 13.

The representative value is here fixed at the average value of the corrosion grade (i.e., $a = 0.5$). The effect of using an alternative representative value is addressed in Appendix B, where it is shown that the value of a is of minor importance compared to effect of the shape (η) for the model used here.

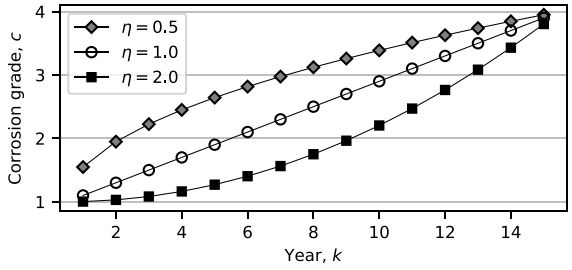

Fig. 13. Example of corrosion grade histories with $C_{\text{end}} = 4$, $L = 15$, $a = 0.5$ and different shape parameters.

Results for mooring line 5 (West) are shown in Fig. 14. With uncertain corrosion grade and linear development (case IIa), the expected fatigue damage is approximately the same as that obtained for the deterministic reference case (which also has a linear development). The uncertainty introduced is reflected through a fatigue damage CoV that grows to about 0.25, and a 97.5-percentile which is roughly 50% higher than the deterministic reference value at the end of the period. The effect of the shape of the time history is clear from the results for cases IIb and IIc. With $\eta = 2$, the slow initial corrosion grade development yields a slower fatigue damage growth than for the other cases. This results in a lower expected value, and a more narrow distribution as reflected by the lower CoV – although the accelerating corrosion growth towards the end of the period lifts the CoV and reduces the relative gap.

The highest expected damage is obtained for the case with $\eta = 0.5$, due to the fast initial corrosion grade growth. This case also results in the widest distribution, represented by the higher CoV and 97.5-percentile. The latter effect is a direct result of the simplified probabilistic model defined in (22) and applied here, which gives a wider corrosion grade distribution (higher upper bound) for the early years with a lower value of the shape parameter (η).

Note that the change in slope which is seen after 1988 in Fig. 14 is a result of the fatigue load history used. The loads are higher in some of the following years than in the first nine years considered (see Fig. 10(c)), and this increases the impact of the corrosion grade and its uncertainty towards the end of the period considered.

4.3. Uncertainty in future fatigue loads

So far, we have assumed that the fatigue loads are known. We will now consider two scenarios with unknown fatigue loads. To isolate the effect of these uncertain fatigue loads, the coefficients of the capacity model are assumed fixed at their mean values, and the corrosion grade is assumed fixed at $g^*_2 = c = 1$. In practice, this implies that the degradation due to corrosion is neglected for the present cases, and

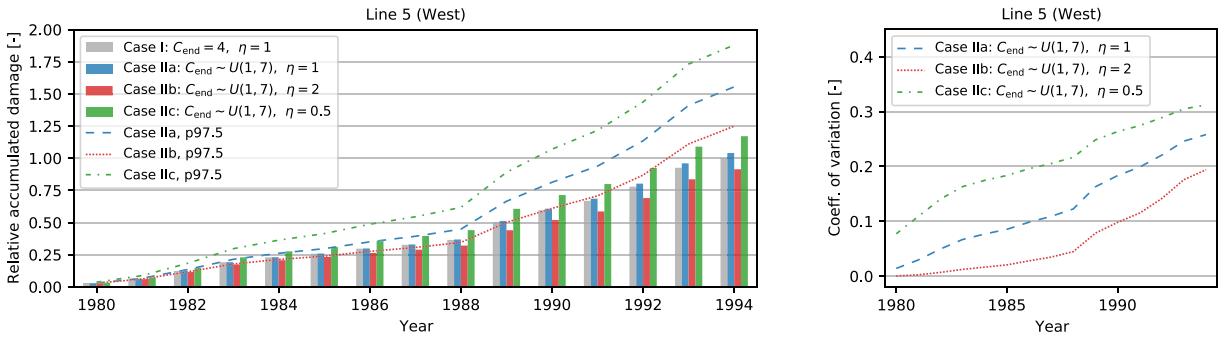

(a) Accumulated fatigue damage: expected value (bars) and 97.5-percentile (lines). Values are normalized wrt. expected damage at end of period for case I.

(b) CoV for accumulated fatigue damage.

Fig. 14. Corrosion grade uncertainty: effect of shape of corrosion history. Mooring line 5 (West).

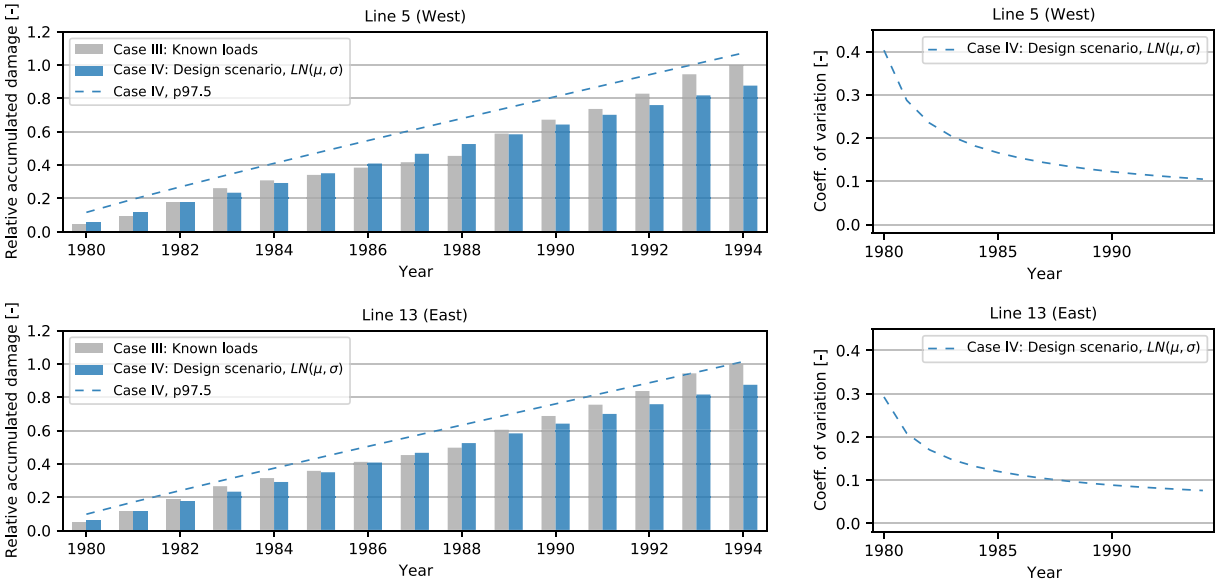

Fig. 15. Fatigue load uncertainty: design verification scenario. Mooring line 5 (upper figures) and 13 (lower).

that the denominator of the fatigue damage summation in (14) becomes constant.

Two distinctly different scenarios are addressed. The first is a *design verification* scenario, where the fatigue loads are uncertain for all the 15 years considered. The distribution of the fatigue loads is assumed known, from the simulations presented in Section 3.[6]

The second scenario is *in-service assessment*. Fatigue loads from $N_p = 10$ prior years are known, whereas the loads in the subsequent $N_f = 5$ future years are uncertain and must be predicted based on inference of the prior loads. Sample statistics for the load variable (Z^*) during the prior years from 1980 to 1989 are listed in Table 5, along with estimated distribution parameters and test-of-fit results to justify a lognormal distribution. Note that the estimated mean value of Z^* agrees quite well with the "true" values (Table 2), whereas the CoV is overestimated for both mooring lines.

Cases to assess the effect of uncertainty in future loads are listed in Table 6. Case III, with known loads for all 15 years, is included as a deterministic reference case. Two cases are defined for the in-service scenario. For case Va, the point-estimates of the distribution parameters are used, thereby neglecting the epistemic uncertainty of the load distribution. This latter uncertainty is addressed with case Vb, applying the bootstrap procedure described in Section 2.7.1.

Note that for the in-service assessment scenario, one could imagine a case where the fatigue load distribution parameters are assumed known initially (as for the design scenario), and either applied "as-is" for the future loads or used as priors for a Bayesian estimation of the posterior distribution of the parameters. Such a case is not considered here.

Results for the design scenario are shown in Fig. 15, and we first consider those for mooring line 5 (upper part of figure). Due to the neglected degradation, the estimated expected fatigue damage for the design case (IV) grows at a constant, annual rate. After nine years (1988), the expected damage is around 15% higher than the reference case. After 15 years, it is roughly 12% on the *low* side, due the high fatigue loads for the reference case in some of the final six years. Still, the final damage of the deterministic case is within the 97.5-percentile of the design case. The results obtained for mooring line 13 are consistent with those for line 5, although with less margin between the estimated 97.5-percentile and the fatigue damage of the reference case.

The CoV plot (Fig. 15(b)) demonstrates a high variability for the initial years, which is significantly reduced to yield a more narrow fatigue damage distribution towards the end of the period. Actually, for this particular case, the fatigue damage is proportional to the sum

[6] This implies that the fatigue loads that are assumed unknown (for the years 1980–1994) are here included in the estimation of the distribution parameters. This inconsistency is disregarded for the sake of this example.

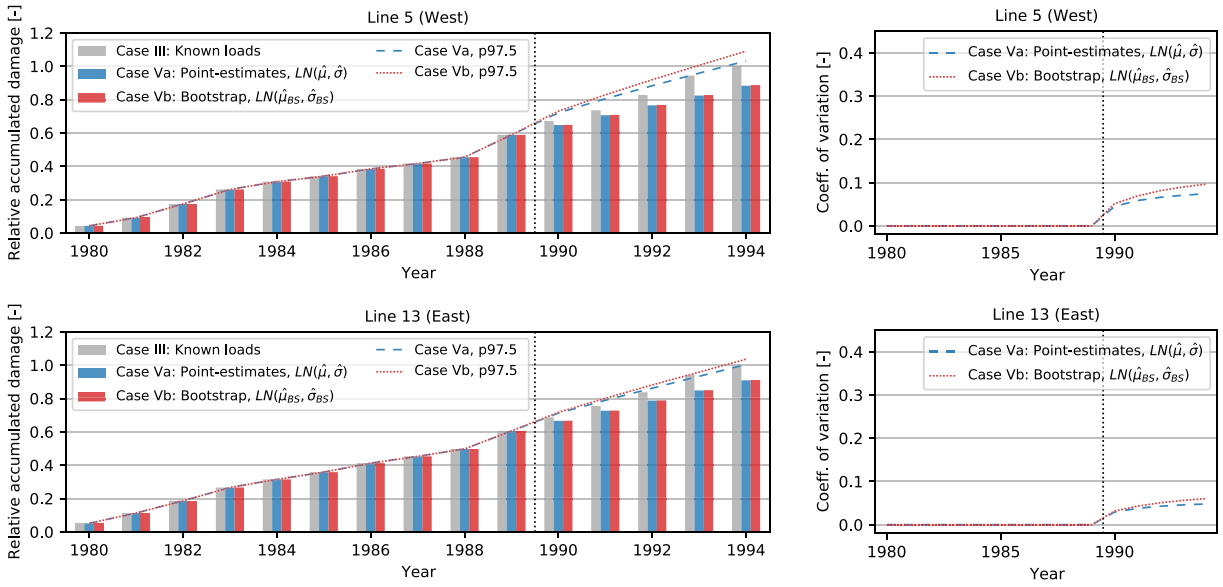

(a) Accumulated fatigue damage: expected value (bars) and 97.5-percentile (lines). Values are normalized wrt. expected damage at end of period for case 1.

(b) CoV for accumulated fatigue damage.

Fig. 16. Fatigue load uncertainty: in-service assessment scenario. Vertical dotted line indicates transition from known to uncertain fatigue loads. Mooring line 5 (upper figures) and 13 (lower).

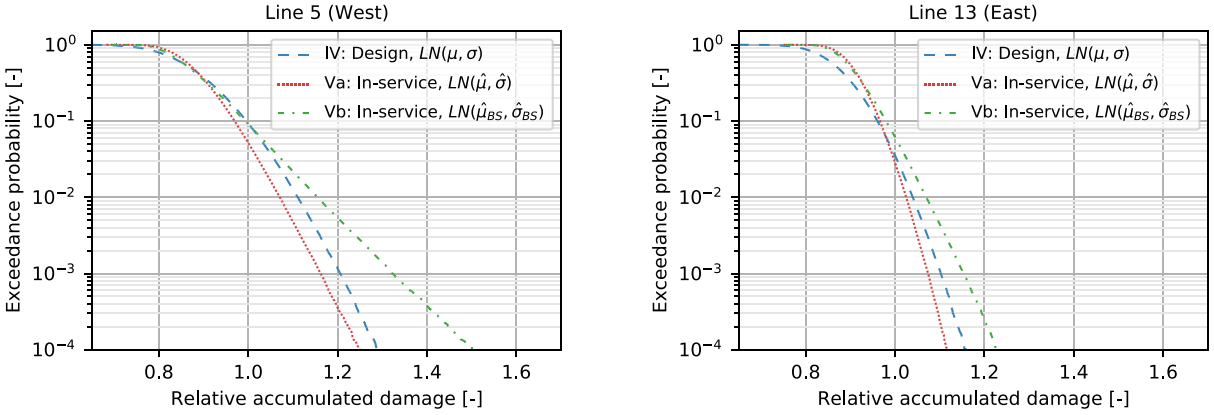

Fig. 17. Probability of exceedance from sample distribution of accumulated fatigue damage after 15 years. Values are normalized wrt. fatigue damage of the reference case with known loads. Mooring lines 5 (left) and 13 (right). Sample size $5{\times}10^5$.

Table 5
Sample statistics, estimated lognormal distribution parameters and test-of-fit results for Z^*. Years 1980–1989.

Line	Cluster	Sample statistics		Fitted parameters		Test statistic [a]		Reject?
		Mean	CoV	$\hat{\mu}$	$\hat{\sigma}$	K–S	A–D	
5	West	$2.61{\times}10^8$	0.55	19.27	0.469	0.249	0.597	No
13	East	$3.49{\times}10^8$	0.35	19.62	0.313	0.188	0.409	No

CoV: Coefficient of Variation; K–S: Kolmogorov–Smirnov test; A–D: Anderson–Darling test.
[a]Critical values (5% level of significance): K–S = 0.409; A–D = 0.685.

Table 6
Cases for assessment of uncertainty in future loads.

Case	Scenario	N_p	N_f	Z^*	Parameters (μ, σ)
III	Reference case	15	0	z_p^*	[a]
IV	Design	0	15	$LN(\mu, \sigma)$	Table 2
Va	In-service	10	5	$LN(\hat{\mu}, \hat{\sigma})$	Table 5
Vb	In-service	10	5	$LN(\hat{\mu}_{BS}, \hat{\sigma}_{BS})$	Bootstrap

[a]Known loads. See Fig. 10(c), years 1980–1994.

of the uncertain and i.i.d. fatigue loads. The temporal evolution of the CoV may therefore be calculated from the relation $V_D^{(N)} = V_{Z^*}/\sqrt{N}$, where $V_D^{(N)}$ is the CoV of accumulated fatigue damage after N years and V_{Z^*} is the CoV of Z^*. This supports the following somewhat intuitive conclusion for the design scenario: both the expected fatigue load and the annual variability are important for the initial years, whereas the mean value is of main importance in the long run. It is emphasized, however, that the degradation due to corrosion is here neglected. The

importance of annual variability for the later years could increase if interaction with uncertain corrosion development is considered.

Results for the in-service cases are shown in Fig. 16. The fatigue loads are deterministic and equal to those of the reference case up to and including the 10th year (1989). After 15 years, the expected fatigue damage is roughly 10% on the low side of the reference case, whereas the 97.5-percentile is around or slightly above it. The CoV is zero for the deterministic part of the simulation. It then increases through the future years (meaning that the standard deviation increases faster than the expected value), but remains on the low side of the design case CoV – despite the higher fatigue load variability for the in-service cases (see CoVs in Table 2 vs. Table 5).

Judging by the CoVs and the 97.5-percentiles in Fig. 16, the bootstrap procedure (case Vb) adds little uncertainty compared to using the point-estimates and neglecting the epistemic uncertainty of the fatigue loads (case Va). As demonstrated by the exceedance plots in Fig. 17, however, it yields a more skewed distribution with a longer upper tail. The difference is small at an exceedance probability of 10^{-1}, but considerably more pronounced at probability level 10^{-3}–10^{-4}. The implication is that the epistemic uncertainty is here of limited importance for the central part of the fatigue damage distribution, whereas it may be of larger importance for problems governed by the tail of the distribution, such as calculation of failure probabilities for mooring lines with a high fatigue reliability.

The exceedance plots also include the sample distributions of the design case. Although not directly comparable to the in-service cases (for which the fatigue load parameter estimation is based on a subset of the data), it still provides an interesting basis for comparison. Firstly; the tail of the sample distribution for in-service case Va is slightly on the low side of the design case, despite its higher fatigue load variability for future years. This is a result of the reduced uncertainty due to knowledge of the fatigue loads in prior years. Secondly; for in-service case Vb, which addresses the epistemic uncertainty of the fatigue load parameters, the tail is on the high side of the design case. This may be interpreted as the cost of not knowing the true distribution parameters, and estimating them from a limited basis. Finally; note that for a different set of cases, the sample distributions of the in-service cases could be shifted either right or left compared to that of the design case, depending on the prior loads, the number of prior years, or the total number of years considered.

4.4. Conclusions of case study

Using deterministic fatigue load and corrosion grade histories, it has been shown that the impact of the inferential uncertainty of the S–N curve coefficients estimated in Lone et al. (2021) is negligible compared to that of the predictive uncertainty of the underlying regression model. This result is used to justify the following simplification of the S–N capacity model: the mean load and corrosion grade effect coefficients (b_1 and b_2, respectively) may be assumed fixed at their respective mean values, whereas the predictive uncertainty is included in the probabilistic description of the b_0 coefficient.

Based on a simple probabilistic corrosion grade model, the impact of uncertain corrosion grade at end of the service life and the shape of the time history have been demonstrated. A faster initial corrosion grade development, with uncertain final value, is seen to increase both the expected value and the CoV of the accumulated fatigue damage compared to a slower initial development.

For the case study presented here, fatigue load uncertainty alone causes a CoV in the range 0.05–0.11 for accumulated fatigue damage after 15 years. This is considerably less than the CoV due to uncertainty in fatigue capacity (0.41) or corrosion grade development (0.19–0.31). However, these quantities and their relative importance could be different for other systems or for alternative cases or quantities of interest; (i) other mooring systems could exhibit larger fatigue load variability or the loads could be found to follow a different probability distribution than the lognormal considered here; (ii) the corrosion grade uncertainty could be reduced through inspection; (iii) the total effect of fatigue load uncertainty could increase if interaction with corrosion grade uncertainty were considered; (iv) the relative importance may be different for the tail of the fatigue damage distribution, which has only been briefly addressed in the present study but could be governing for calculation of failure probability.

5. Conclusions

A new probabilistic model for mooring chain fatigue has been developed, based on a S–N formulation with parameterized dependence to mean load and corrosion grade. Time dependencies of underlying random variables are handled by expressing the accumulated fatigue damage as a sum of time-invariant contributions. Owing to the introduction of representative values for the mean load and corrosion grade functions, this piecewise time-invariant formulation represents only a minor inaccuracy compared to a fully time-variant one.

The model enables accounting for the uncertain and temporal development of corrosion, as well as the variability of both mean loads and cyclic fatigue loads. To account for the correlation between the latter two loads it is proposed that they are combined into a single random variable. A necessary condition for this measure to be taken is that the mean load effect on the fatigue capacity is assumed to be deterministic. By distinguishing between the fatigue damage due to prior known loads and that caused by future uncertain loads, the utilization of load history from prior operation is enabled. This way, uncertainties that were present at the design stage may be reduced in connection with in-service assessment of the mooring system fatigue performance.

Mooring line response simulations have been performed for a realistic mooring system in the Norwegian Sea, based on a long series of hindcast data. Results from these simulations have been presented and discussed in light of the probabilistic model, and then used as the basis for a case study. Based on our model, the case study demonstrated the isolated effects of uncertainty in capacity, corrosion and fatigue loads on the distribution of accumulated fatigue damage.

Future work. Although the model implicitly handles the interaction between corrosion grade uncertainty and fatigue load variability, this has not been explicitly addressed or quantified in the present study. The case study results do, however, suggest that such interaction could be of some importance. For future work, this could be quantified by means of for instance a global sensitivity analysis, using variance decomposition techniques (Saltelli et al., 2008).

A probabilistic fatigue damage model forms the basis for reliability analysis to calculate the probability of mooring line fatigue failure. In addition to the uncertainties addressed explicitly in the present study, such analysis needs to take into account model uncertainties addressing inaccuracies and possible bias introduced by the underlying mathematical models and inaccurate data. Examples relevant for the current model include: the use of a S–N model to represent the fatigue effect; load measurements; numerical mooring system model and environmental data (when load history stems from simulations); the use of a parametric distribution to represent future loads. Furthermore, a mooring system does not consist of a single chain component, as considered here, but of several lines that may each be composed of multiple segments with typically 100+ components each. A reliability analysis must reflect that fatigue failure in any of these components leads to a mooring line failure.

CRediT authorship contribution statement

Erling N. Lone: Conceptualization, Methodology, Software, Formal analysis, Data curation, Visualization, Writing – original draft, Writing – review & editing. **Thomas Sauder:** Conceptualization, Writing –

review & editing, Supervision. **Kjell Larsen:** Conceptualization, Writing – review & editing, Supervision. **Bernt J. Leira:** Conceptualization, Writing – review & editing, Supervision, Funding acquisition.

Declaration of competing interest

The authors declare that they have no known competing financial interests or personal relationships that could have appeared to influence the work reported in this paper.

Acknowledgments

This study was financed by the Research Council of Norway, through the project 280705 "Improved lifetime estimation of mooring chains" (LIFEMOOR). Marit Kvittem (SINTEF Ocean) is acknowledged for conducting the hindcast-based simulations that provide the basis for the case study.

Appendix A. Goodness-of-fit tests for lognormal distribution of Z and Z^*

Goodness-of-fit tests have been performed to assess the validity of the assumption that the fatigue load variables Z and Z^* follow a lognormal distribution. Two different tests have been applied: (i) the Kolmogorov–Smirnov (K–S) test, which considers the maximum discrepancy between the empirical and theoretical (fitted) distribution functions, and (ii) the Anderson–Darling (A–D) test, which places more weight in the tails of the distribution. For details on these test procedures, see e.g., Ang and Tang (2007).

Annual data from all 61 years of simulations is considered, with lognormal distribution parameters (μ, σ) estimated from Eqs. (17) and (18). Results are listed in Table A.7, along with critical values for significance level 5%. The calculated test statistics are below the critical value for both tests, for both response variables and all mooring lines considered. Therefore, the lognormal distribution is acceptable at the 5% level of significance.

Probability paper plots are presented in Fig. A.18, for comparison of the empirical and fitted distributions for lines 5 and 13. The plots demonstrate good agreement for the central part of the distributions for both response variables. Some discrepancies are observed in the right tail, with the empirical distribution on the high side. This indicates that the fitted lognormal distribution may be non-conservative in the upper tail region, but the plots give limited basis as to conclude whether the deviations are caused by statistical uncertainty or systematic bias. In any case, as fatigue damage is accumulated over several years the exact tail behavior of the annual load distribution becomes less important compared to the overall fit. Minor emphasis is therefore placed on the observed discrepancies, as long as the test-of-fit results are acceptable.

Appendix B. Effect of choice of representative value for corrosion grade function

The effect of choice of representative value for the corrosion grade is considered, using known fatigue loads and a linear corrosion grade development ($\eta = 1$). Two cases are compared: corrosion grade function is represented by the its final value in each year ($a = 0$), versus using the average value ($a = 0.5$). The latter is identical to case IIa of the case study (see Section 4.2, Table 4).

Results are shown in Fig. B.19. When the final value is used ($a = 0$), the fatigue damage increases compared to when the average value is used ($a = 0.5$). The differences are small, however, with less than 2% increase for the CoV and only 3%–4% for the expected damage and 97.5-percentile. Furthermore, the impact of different representative values is small compared to that of different shapes (cf. Fig. 14). On this basis, the average value seems like a reasonable choice for the representative value, since using the final value for each year is demonstrably conservative. However, larger differences could result for a different probabilistic model or if an alternative corrosion grade function ($g_2(c)$) was used.

Nomenclature

E[.]	Mathematical expectation
ln(.)	Natural logarithm
log(.)	Common logarithm
$\sim$	distributed as
$LN(\mu, \sigma)$	Lognormal distribution with scale parameter $\exp\{\mu\}$ and shape parameter σ
$N(\mu, \sigma^2)$	Normal distribution with mean μ and variance σ^2
$U(a, b)$	Uniform distribution with support $[a, b]$
η	Exponent of probabilistic corrosion model, see (22)
$\hat{\mu}$	Maximum likelihood estimate of μ
$\hat{\sigma}$	Maximum likelihood estimate of σ
μ	Mean value Logarithm of scale parameter of lognormal distribution
σ	Standard deviation Shape parameter of lognormal distribution
σ_m	Mean stress [MPa]
σ_ε	Standard error of regression model
ε	Regression error, see (19)
a	Variable of probabilistic corrosion model, support $[0, 1]$, see (22)
$A(\sigma_m, c)$	Mean load and corrosion dependent intercept parameter of S–N curve, see (3)
b_0	Coefficient of S–N curve intercept parameter, see (3)
b_1	Coefficient of S–N curve intercept parameter (mean load effect), see (3)
b_2	Coefficient of S–N curve intercept parameter (corrosion grade effect), see (3)
c	Corrosion grade, support $[1, 7]$
C_{end}	Corrosion grade at end of service life, see (22)
D	Fatigue damage (Palmgren–Miner sum)
$g_1(\sigma_m)$	Mean load function, see (3)
g_1^*	Representative value of mean load function over a specified period, see (10)
$g_2(c)$	Corrosion grade function, see (3)
g_2^*	Representative value of corrosion grade function over a specified period
m	Slope parameter of S–N curve
N	Number of cycles to failure, see (1) Sample size for estimation of distribution parameters, see (17) and (18)
N_f	Number of future years
N_p	Number of prior years
N_T	Total number of years
N_{MC}	Sample size (number of realizations) generated in Monte Carlo simulation
S	Stress range [MPa]
Z	Fatigue load, see (11)
Z^*	Fatigue load including mean load effect, see (12)
z_p, z_p^*	Realization of prior fatigue loads
CoV	Coefficient of Variation
i.i.d.	independent and identically distributed
MCS	Monte Carlo Simulation

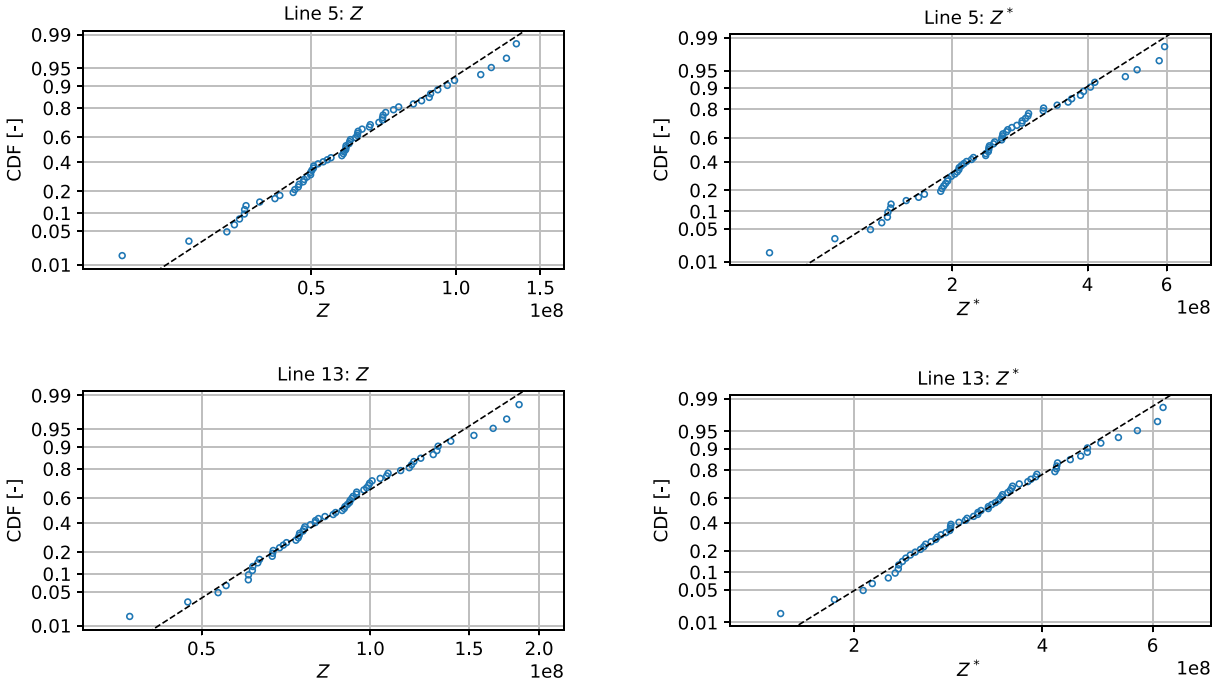

Fig. A.18. Empirical (markers) vs. fitted (dashed) distributions for Z (left) and Z^* (right) on lognormal probability paper. Simulation data for 61 years (1958–2918). Mooring lines 5 (upper) and 13 (lower).

Table A.7
Test-of-fit results for lognormal distribution, at 5% level of significance. Based on simulations for 61 years.

Variable, Mooring line	Cluster	Fitted parameters		K–S test			A–D test		
		$\hat{\mu}$	$\hat{\sigma}$	Test statistic	Critical value	Reject?	Test statistic	Critical value	Reject?
$Z = n_0 \cdot \mathrm{E}[S^m]$									
1	South	18.23	0.257	0.057	0.171	No	0.257	0.741	No
5	West	17.88	0.364	0.075	0.171	No	0.390	0.741	No
9	North	18.11	0.235	0.095	0.171	No	0.644	0.741	No
13	East	18.29	0.316	0.066	0.171	No	0.238	0.741	No
$Z^* = n_0 \cdot \mathrm{E}[S^m] \cdot 10^{-b_1 \cdot g_i^*}$									
1	South	19.72	0.282	0.064	0.171	No	0.232	0.741	No
5	West	19.30	0.389	0.083	0.171	No	0.408	0.741	No
9	North	19.59	0.252	0.093	0.171	No	0.714	0.741	No
13	East	19.59	0.287	0.062	0.171	No	0.192	0.741	No

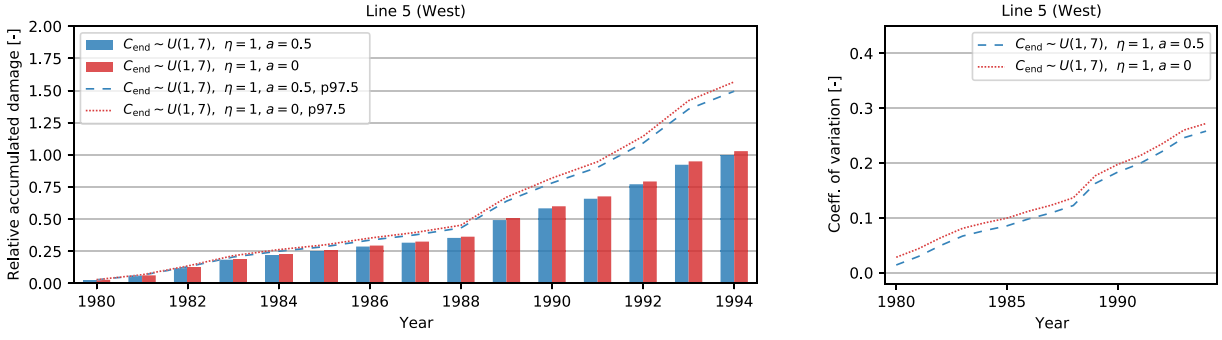

(a) Accumulated fatigue damage: expected value (bars) and 97.5-percentile (lines). Values are normalized wrt. expected damage at end of period for the case with $a = 0.5$.

(b) CoV for accumulated fatigue damage.

Fig. B.19. Corrosion grade uncertainty: effect of choice of representative value. Mooring line 5 (West).

References

Ang, A.H.-S., Tang, W.H., 2007. Probability Concepts in Engineering: Emphasis on Applications in Civil & Environmental Engineering, second ed. Wiley, New York.

ASTM International, 2017. Standard practices for cycle counting in fatigue analysis (ASTM 1049-85), Reapproved 2017. http://dx.doi.org/10.1520/E1049-85R17.2.

Brown, M.G., Hall, T.D., Marr, D.G., English, M., Snell, R.O., 2005. Floating production mooring integrity JIP - key findings. In: Offshore Technology Conference. Houston, Texas, p. 12. http://dx.doi.org/10.4043/17499-MS.

Burnham, K.P., Anderson, D.R., 2002. Model Selection and Multimodel Inference, second ed. Springer New York, New York, NY, http://dx.doi.org/10.1007/b97636.

Bury, K., 1999. Statistical Distributions in Engineering. Cambridge University Press, http://dx.doi.org/10.1017/CBO9781139175081.

Christiansen, N.H., 2014. Hybrid method simulation of slender marine structures. (Ph.D. thesis). DTU Mechanical Engineering, URL https://orbit.dtu.dk/en/publications/hybrid-method-simulation-of-slender-marine-structures.

DNV GL, 2018. Offshore Standard - Position mooring (DNVGL-OS-E301), Edition July 2018.

DNV GL, 2019. Recommended Practice - Environmental conditions and environmental loads (DNVGL-RP-C205), Edition September 2019.

Efron, B., 2012. Bayesian inference and the parametric bootstrap. Ann. Appl. Stat. 6 (4), http://dx.doi.org/10.1214/12-AOAS571.

Efron, B., Tibshirani, R., 1986. Bootstrap methods for standard errors, confidence intervals, and other measures of statistical accuracy. Statist. Sci. 1 (1), 54–75. http://dx.doi.org/10.1214/ss/1177013815.

Fernández, J., Arredondo, A., Storesund, W., González, J.J., 2019. Influence of the mean load on the fatigue performance of mooring chains. In: Proceedings of the Annual Offshore Technology Conference. OTC-29621-MS, http://dx.doi.org/10.4043/29621-MS.

Fernández, J., Storesund, W., Navas, J., 2014. Fatigue performance of grade R4 and R5 mooring chains in seawater. In: Proceedings of the ASME 2014 33rd International Conference on Ocean, Offshore and Arctic Engineering. OMAE2014-23491, http://dx.doi.org/10.1115/OMAE2014-23491.

Fontaine, E., Kilner, A., Carra, C., Washington, D., Ma, K.T., Phadke, A., Laskowski, D., Kusinski, G., 2014. Industry survey of past failures, pre-emptive replacements and reported degradations for mooring systems of floating production units. In: Offshore Technology Conference. OTC-25273-MS, Houston, Texas, http://dx.doi.org/10.4043/25273-MS.

Fredheim, S., Reinholdtsen, S.-A., Håskoll, L., Lie, H.B., 2013. Corrosion fatigue testing of used, studless, offshore mooring chain. In: Proceedings of the ASME 2013 32nd International Conference on Ocean, Offshore and Arctic Engineering. OMAE2013-10609.

Gabrielsen, Ø., Larsen, K., Dalane, O., Lie, H.B., Reinholdtsen, S.-A., 2019. Mean load impact on mooring chain fatigue capacity: Lessons learned from full scale fatigue testing of used chains. In: Proceedings of the ASME 2019 38th International Conference on Ocean, Offshore and Arctic Engineering. OMAE2019-95083, http://dx.doi.org/10.1115/OMAE2019-95083.

Gabrielsen, Ø., Larsen, K., Reinholdtsen, S.A., 2017. Fatigue testing of used mooring chain. In: Proceedings of the ASME 2017 36th International Conference on Ocean, Offshore and Arctic Engineering. OMAE2017-61382, http://dx.doi.org/10.1115/OMAE2017-61382.

Gelman, A., Hill, J., 2007. Data Analysis using Regression and Multilevel/Hierarchical Models. In: Analytical methods for social research, Cambridge University Press, Cambridge, http://dx.doi.org/10.1017/CBO9780511790942.

Hastie, T., Tibshirani, R., Friedman, J., 2001. the Elements of Statistical Learning - Data Mining, Inference, and Prediction. In: Springer Series in Statistics, Springer New York, New York, NY, http://dx.doi.org/10.1007/978-0-387-21606-5.

Hørte, T., Russo, M., Macke, M., Reinås, L., 2013. Benefit of measurements and structural reliability analysis for wellhead fatigue. In: Proceedings of the ASME 2013 32nd International Conference on Ocean, Offshore and Arctic Engineering. OMAE2013-10932, American Society of Mechanical Engineers, Nantes, France, http://dx.doi.org/10.1115/OMAE2013-10932.

ISO 19901-1, 2015. Petroleum and natural gas industries - Specific requirements for offshore structures - Part 1: Metocean design and operating considerations. International Organization for Standardization.

ISO 19901-7, 2013. Petroleum and Natural Gas Industries - Specific Requirements for Offshore Structures - Part 7: Stationkeeping Systems for Floating Offshore Structures and Mobile Offshore Units, Second ed. International Organization for Standardization.

Kvitrud, A., 2014. Lessons learned from norwegian mooring line failures 2010–2013. In: Proceedings of the ASME 2014 33rd International Conference on Ocean, Offshore and Arctic Engineering. http://dx.doi.org/10.1115/OMAE2014-23095.

Lone, E.N., Leira, B.J., Sauder, T., Aksnes, V., Gabrielsen, Ø., Larsen, K., 2020. Influence of mean tension on mooring line fatigue life. In: Proceedings of the ASME 2020 39th International Conference on Ocean, Offshore and Arctic Engineering, Virtual. OMAE2020-18628, http://dx.doi.org/10.1115/OMAE2020-18628.

Lone, E.N., Sauder, T., Larsen, K., Leira, B.J., 2021. Fatigue assessment of mooring chain considering the effects of mean load and corrosion. In: Proceedings of the ASME 2021 40th International Conference on Ocean, Offshore and Arctic Engineering, Virtual. OMAE2021-62775, http://dx.doi.org/10.1115/OMAE2021-62775.

Ma, K.-t., Gabrielsen, Ø., Li, Z., Baker, D., Yao, A., Vargas, P., Luo, M., Izadparast, A., Arredondo, A., Zhu, L., Sverdlova, N., Høgsæt, I.S., 2019. Fatigue tests on corroded mooring chains retrieved from various fields in offshore west africa and the north sea.. In: Proceedings of the ASME 2019 38th International Conference on Ocean, Offshore and Arctic Engineering. OMAE2019-95618, Glasgow, Scotland, UK, http://dx.doi.org/10.1115/OMAE2019-95618.

Ma, K.-t., Shu, H., Smedley, P., L'Hostis, D., Duggal, A., 2013. A historical review on integrity issues of permanent mooring systems. In: Offshore Technology Conference. OTS-24025-MS, Houston, Texas, USA, http://dx.doi.org/10.4043/24025-MS.

Melchers, R.E., Beck, A.T., 2018. Structural Reliability Analysis and Prediction, third ed. John Wiley & Sons, Inc., Hoboken, NJ.

Moan, T., Gao, Z., Ayala-Uraga, E., 2005. Uncertainty of wave-induced response of marine structures due to long-term variation of extratropical wave conditions. Mar. Struct. 18 (4), 359–382. http://dx.doi.org/10.1016/j.marstruc.2005.11.001.

O'Connor, A., Modarres, M., Mosled, A., 2007. Probability Distributions Used in Reliability Engineering. Center for Risk and Reliability, University of Maryland, p. 219, https://crr.umd.edu/sites/crr.umd.edu/files/FreeEbookProbabilityDistributionsUsedinReliabilityEngineeringpdf.

Ormberg, H., Larsen, K., 1998. Coupled analysis of floater motion and mooring dynamics for a turret-moored ship. Appl. Ocean Res. 20 (1–2), 55–67. http://dx.doi.org/10.1016/S0141-1187(98)00012-1.

Ormberg, H., Sødahl, N., Steinkjer, O., 1998. Efficient analysis of mooring systems using de-coupled and coupled analysis. In: Proceedings of the 17th International Conference on Ocean, Offshore Mechanics and Arctic Engineering.

Reistad, M., Breivik, Ø., Haakenstad, H., Aarnes, O.J., Furevik, B.R., Bidlot, J.-R., 2011. A high-resolution hindcast of wind and waves for the North sea, the Norwegian sea, and the Barents sea. J. Geophys. Res. Oceans 116 (C05019), 1–18. http://dx.doi.org/10.1029/2010JC006402.

Renzi, D., Maniar, D., McNeill, S., Del Vecchio, C., 2017. Developing a digital twin for floating production systems integrity management. In: Proceedings of the Annual Offshore Technology Conference. OTC-28012-MS, OTC, pp. 1734–1741. http://dx.doi.org/10.4043/28012-MS.

Russo, M., Holden, H., Reinås, L., Sæther, M., 2012. Fatigue assessment of subsea wells for future and historical operations based on measured riser loads. In: Proceedings of the ASME 2012 31st International Conference on Ocean, Offshore and Arctic Engineering. OMAE2012-83162, pp. 139–150. http://dx.doi.org/10.1115/OMAE2012-83162.

Saltelli, A., Ratto, M., Andres, T., Campolongo, F., Cariboni, J., Gatelli, D., Saisana, M., Tarantola, S., 2008. Global Sensitivity Analysis. The Primer. John Wiley & Sons, Ltd, Chichester, UK, http://dx.doi.org/10.1002/9780470725184.

SINTEF Ocean, 2019a. SIMO Theory Manual Version 4.17.

SINTEF Ocean, 2019b. RIFLEX Theory Manual Version 4.17.

Steinkjer, O., Sødahl, N., Grytøyr, G., 2010. Methodology for time domain fatigue life assessment of risers and umbilicals. In: Proceedings of the ASME 2010 29th International Conference on Ocean, Offshore and Arctic Engineering. OMAE2010-20119, http://dx.doi.org/10.1115/OMAE2010-20119.

Torsethaugen, K., Haver, S., 2004. Simplified double peak spectral model for ocean waves. In: Proceedings of the Fourteenth International Offshore and Polar Engineering Conference, Toulon, pp. 76–84.

Wirsching, P.H., Chen, Y.N., 1988. Considerations of probability-based fatigue design for marine structures. Mar. Struct. 1 (1), 23–45. http://dx.doi.org/10.1016/0951-8339(88)90009-3.

Zhang, Y., Smedley, P., 2019. Fatigue performance of high strength and large diameter mooring chain in seawater. In: Proceedings of the ASME 2019 38th International Conference on Ocean, Offshore and Arctic Engineering. OMAE2019-95984, Glasgow, Scotland, UK, http://dx.doi.org/10.1115/OMAE2019-95984.

Zhao, Y., Dong, S., Jiang, F., Incecik, A., 2021. Mooring tension prediction based on BP neural network for semi-submersible platform. Ocean Eng. 223, 108714. http://dx.doi.org/10.1016/j.oceaneng.2021.108714.